



THE UNIVERSITY *of* EDINBURGH

Edinburgh Research Explorer

A mechanism for the suppression of homologous recombination in G1 cells

Citation for published version:

Orthwein, A, Noordermeer, SM, Wilson, MD, Landry, S, Enchev, RI, Sherker, A, Munro, M, Pinder, J, Salsman, J, Dellaire, G, Xia, B, Peter, M & Durocher, D 2015, 'A mechanism for the suppression of homologous recombination in G1 cells', *Nature*, vol. 528, no. 7582, pp. 422-426.
<https://doi.org/10.1038/nature16142>

Digital Object Identifier (DOI):

[10.1038/nature16142](https://doi.org/10.1038/nature16142)

Link:

[Link to publication record in Edinburgh Research Explorer](#)

Document Version:

Peer reviewed version

Published In:

Nature

General rights

Copyright for the publications made accessible via the Edinburgh Research Explorer is retained by the author(s) and / or other copyright owners and it is a condition of accessing these publications that users recognise and abide by the legal requirements associated with these rights.

Take down policy

The University of Edinburgh has made every reasonable effort to ensure that Edinburgh Research Explorer content complies with UK legislation. If you believe that the public display of this file breaches copyright please contact openaccess@ed.ac.uk providing details, and we will remove access to the work immediately and investigate your claim.



Induction of homologous recombination in G1 cells

Nature manuscript 2015-02-02648B

Alexandre Orthwein^{1*}, Sylvie M. Noordermeer^{1*}, Marcus D. Wilson¹, Sébastien Landry¹, Radoslav I. Enchev³, Alana Sherker^{1,2}, Meagan Munro¹, Jordan Pinder⁴, Graham Dellaire⁴, Bing Xia⁵, Matthias Peter³ and Daniel Durocher^{1,2,¶}

¹The Lunenfeld-Tanenbaum Research Institute, Mount Sinai Hospital, 600 University Avenue, Toronto, ON, M5G 1X5, Canada

²Department of Molecular Genetics, University of Toronto, ON, M5S 3E1, Canada.

³ETH Zurich, Institute of Biochemistry, Department of Biology, Otto-Stern-Weg 3, CH-8093 Zurich, Switzerland.

⁴Departments of Pathology and Biochemistry & Molecular Biology, Dalhousie University, Halifax, Nova Scotia, B3H 4R2, Canada

⁵Department of Radiation Oncology, Rutgers Cancer Institute of New Jersey and Robert Wood Johnson Medical School, Rutgers, The State University of New Jersey, New Brunswick, New Jersey, USA

*These authors contributed equally to this work.

Format: Nature Letter

¶Address correspondence to:

Daniel Durocher, Ph.D.
The Lunenfeld-Tanenbaum Research Institute
Mount Sinai Hospital, Room 1073
600 University Avenue
Toronto, ON M5G 1X5
CANADA
Tel: 416-586-4800 ext. 2544
e-mail: durocher@lunenfeld.ca

DNA repair by homologous recombination (HR)¹ is highly suppressed in G1 cells^{2,3} to ensure that mitotic recombination occurs solely between sister chromatids^{4,5}. Although many HR factors are cell cycle-regulated, the identity of the key events that are both necessary and sufficient to suppress recombination in G1 cells is unknown. Here we report that the cell cycle tightly controls the interaction of BRCA1 with PALB2-BRCA2 in order to constrain BRCA2 function to the S/G2 phases. We found that the BRCA1-interaction site on PALB2 is targeted by an E3 ubiquitin ligase composed of KEAP1, a PALB2-interacting protein⁶, in complex with CUL3⁷. PALB2 ubiquitylation suppresses its interaction with BRCA1 and is counteracted by the deubiquitylase USP11, which is itself under cell cycle control. We conclude that suppression of BRCA1-PALB2-BRCA2 complex assembly is a critical component of the regulatory network that prohibits recombination in G1 cells. Indeed, restoration of the BRCA1-PALB2 interaction combined with the activation of DNA end resection is sufficient to induce HR in G1, as measured by RAD51 recruitment, unscheduled DNA synthesis and a CRISPR/Cas9-based gene targeting assay. The ability to induce HR in G1 cells with defined factors could represent a stepping-stone for the development of gene targeting applications in non-dividing cells.

The breast and ovarian tumour suppressors BRCA1, PALB2 and BRCA2 promote DNA double-strand break (DSB) repair by HR⁸⁻¹⁰. BRCA1 acts in this process minimally at two steps. Firstly, it promotes DNA end resection^{11,12}, the initiating step in HR that involves the nucleolytic processing of breaks to produce the single-stranded (ss) DNA necessary for homology search and strand invasion¹. Secondly, BRCA1 interacts with PALB2¹³⁻¹⁵ to direct the recruitment of BRCA2¹³ and RAD51^{16,17} to DSB sites. The accumulation of BRCA1 on the chromatin that

flanks DSB sites is strikingly suppressed in G1 cells¹⁸, reminiscent of the potent inhibition of HR in this phase of the cell cycle. Since the inhibition of BRCA1 recruitment in G1 is dependent on the 53BP1 and RIF1 proteins^{18,19}, two inhibitors of end-resection¹⁸⁻²², this regulation of BRCA1 was originally viewed in light of its function in stimulating DNA end processing.

However, as BRCA1 is also involved in promoting the recruitment of BRCA2 through its interaction with PALB2¹³⁻¹⁵, we asked whether inducing BRCA1 recruitment to DSB sites in G1, through mutation of *53BP1* by genome editing (*53BP1*Δ; [Extended Data Fig. 1a-c](#)) also resulted in BRCA2 accumulation into ionizing radiation (IR)-induced foci. To our surprise, we found that in contrast to BRCA1 neither BRCA2 nor PALB2 are recruited to G1 DSB sites in U-2-OS (U2OS) cells lacking 53BP1 at IR doses ranging from 2 to 20 Gy ([Fig. 1ab](#) and [Extended Data Fig. 1de](#)). Since BRCA1 and PALB2 interact directly^{13,14}, this result suggested that G1 cells may block BRCA2 recruitment by suppressing the BRCA1-PALB2 interaction. Indeed, while PALB2 interacts with BRCA2 irrespective of cell cycle position, it interacted efficiently with BRCA1 only during S phase ([Fig. 1c](#)). The presence of DNA damage led to the loss of the residual PALB2-BRCA1 interaction in G1 whereas it had little impact on the assembly of the BRCA1-PALB2-BRCA2 complex in S phase ([Fig. 1c](#)). Since all proteins were expressed in G1 ([Fig. 1c](#)), our results suggest that the assembly of the BRCA1-PALB2-BRCA2 complex is controlled during the cell cycle, possibly to restrict the accumulation of BRCA2 at DSB sites to the S/G2 phases.

We confirmed these results using a single-cell assay assessing the co-localization, at an integrated *LacO* array²³, of an mCherry-tagged LacR-BRCA1 fusion protein with GFP-tagged PALB2 ([Extended Data Fig. 2a](#)). This LacR/*LacO* system recapitulated the cell cycle-dependent and DNA damage-sensitive BRCA1-PALB2 interaction ([Extended Data Fig. 2b](#)) and enabled us

to determine that sequences on PALB2, located outside its N-terminal BRCA1-interaction domain (residues 1-50) were responsible for the cell cycle-dependent regulation of its association with BRCA1 (Extended Data Fig. 2cd). Further deletion mutagenesis identified a single region, encompassed within residues 46-103 in PALB2 (Extended Data Fig. 2ef) responsible for the cell cycle-dependent regulation of the BRCA1-PALB2 interaction. This region corresponds to the interaction site for KEAP1⁶, identifying this protein as a candidate regulator of the BRCA1-PALB2 interaction.

KEAP1 is a substrate adaptor for a CRL3 E3 ubiquitin (Ub) ligase that targets the antioxidant regulator NRF2 for proteasomal degradation²⁴ and recognizes an “ETGE” motif on both PALB2 and NRF2 through its KELCH domain⁶. Depletion of KEAP1 from *53BP1Δ* cells, or deletion of the ETGE motif in full-length PALB2 (PALB2 ΔETGE) induced G1-phase PALB2 IR-induced focus formation (Fig 1d and Extended Data Fig. 3a). Furthermore, in cells in which *KEAP1* was inactivated by genome editing (*KEAP1Δ*, Extended Data Fig. 3b) we detected a stable BRCA1-PALB2-BRCA2 complex in both G1 and S phases (Fig. 1e). KEAP1 is therefore an inhibitor of the BRCA1-PALB2 interaction.

CUL3 also interacts with PALB2 (Extended Data Fig. 3c) and its depletion in *53BP1Δ* U2OS cells de-repressed PALB2 IR-induced foci in G1 (Fig. 1d and Extended Data Fig. 3a). Furthermore, in G1-synchronized *KEAP1Δ* cells, expression of a CUL3-binding deficient KEAP1 protein that lacks its BTB domain (ΔBTB) failed to suppress the BRCA1-PALB2 interaction, unlike its wild type counterpart (Fig. 1f). These results suggest that KEAP1 recruits CUL3 to PALB2 to suppress its interaction with BRCA1.

Using the LacR/*LacO* system and co-immunoprecipitation assays, we found that a mutant of PALB2 lacking all 8 lysine residues in the BRCA1-interaction domain (PALB2-KR; Fig 2a)

could interact with BRCA1 irrespective of cell cycle position (Fig. 2b and Extended Data Fig. 3de). Further mutagenesis identified residues 20, 25 and 30 in PALB2 as critical for the suppression of the BRCA1-PALB2 interaction since re-introduction of these lysines in the context of PALB2-KR (yielding PALB2-KR/K3; Fig 2a) led to the suppression of BRCA1-PALB2-BRCA2 complex assembly in G1 cells (Fig. 2b and Extended Data Fig. 3d). Together, these results suggested a model whereby PALB2-bound KEAP1 forms an active CRL3 complex that ubiquitylates the PALB2 N-terminus to suppress its interaction with BRCA1.

While PALB2 ubiquitylation can be detected in cells (Extended Data Fig. 4a), the lysine-rich nature of the PALB2 N-terminus has so far precluded us from unambiguously mapping in vivo ubiquitylation sites on Lys20, 25 or 30. However we could detect ubiquitylation on Lys16 and Lys43 by mass spectrometry, indicating that the PALB2 N-terminus is ubiquitylated (Extended Data Fig. 4b). In a complementary set of experiments, PALB2 targeted to the *LacO* array induced immunoreactivity to conjugated ubiquitin (Fig 2cd and Extended Data Fig. 4c). Ub colocalization with PALB2 was highest in G1, depended on the KEAP1-interaction motif and the presence of the Lys20/25/30 residues (Fig 2d and Extended Data Fig. 4c), consistent with a model that PALB2 is ubiquitylated on those sites in G1 cells. Indeed, we could readily reconstitute ubiquitylation of the N-terminus of PALB2 (residues 1-103; fused to a HA epitope tag), by recombinant CRL3-KEAP1, in a manner that depended on the KEAP1-interaction domain of PALB2 (Fig. 2e) and we unambiguously identified Lys25 and Lys30 as being ubiquitylated by KEAP1 in vitro by mass spectrometry (Extended Data Fig. 5).

Ubiquitylation of PALB2 by CRL3-KEAP1 inhibited its interaction with BRCA1, which was more obvious with the highly modified forms of PALB2 due to the presence of ubiquitylated lysines outside the BRCA1-interaction domain (Fig. 2f). In order to specifically test whether

ubiquitylation of a single lysine residue of the three identified as critical inhibited the interaction with BRCA1, we used dichloroacetone crosslinking to install a single ubiquitin moiety at position 20 or 45 (yielding PALB2-K_C20-Ub and PALB2-K_C45-Ub). Ubiquitylation of PALB2 at position 20 completely suppressed its interaction with BRCA1 whereas modification of residue 45 had no impact on the interaction ([Extended Data Fig. 6](#)). Together, these results indicate that PALB2 ubiquitylation on specific sites on its N-terminus prevents its interaction with BRCA1.

Since neither the activity of the CRL3-KEAP1 E3 ligase ([Extended Data Fig. 7](#)) nor the interaction of CRL3-KEAP1 with PALB2 ([Extended Data Fig. 3c](#)) are regulated by the cell cycle, we considered the possibility that deubiquitylation of PALB2 might be regulated in a cell cycle-dependent manner. KEAP1 physically interacts with USP11²⁵, a deubiquitylase that also interacts with BRCA2²⁶ and PALB2 ([Extended Data Fig. 8a](#)). USP11 depletion impairs gene conversion²⁷ ([Extended Data Fig. 8b](#)) and results in hypersensitivity to PARP inhibition²⁷ identifying it as an HR regulator of unknown function. Co-immunoprecipitation experiments confirmed that USP11 and its catalytic activity were necessary for the formation of a stable BRCA1-PALB2-BRCA2 complex, especially in the presence of DNA damage ([Fig. 3a](#) and [Extended Data Fig. 8cd](#)).

If USP11 antagonizes PALB2 ubiquitylation by CRL3-KEAP1, then removal of KEAP1 (or CUL3) should reverse the phenotypes imparted by loss of USP11. Indeed, deletion of KEAP1 restored PARPi resistance and the BRCA1-PALB2 interaction in USP11 knockout cells prepared by genome editing (*USP11Δ*) ([Fig 3bc](#) and [Extended Data Fig. 8c](#)). Likewise, depletion of CUL3 or KEAP1 reversed the gene conversion defect of USP11-depleted cells ([Extended Data Fig. 9a](#)). Introduction of the PALB2-KR mutant restored its interaction with BRCA1 and reversed PARPi

sensitivity in *USP11Δ* cells in a manner that depended on Lys20/25/30 (Extended Data Fig. 9bc). Since recombinant USP11 can directly de-ubiquitylate PALB2 (1-103) (Fig. 3d), these results suggest that USP11 promotes the assembly of the BRCA1-PALB2-BRCA2 complex by reversing ubiquitylation on the PALB2 Lys20/25/30 residues.

We observed that USP11 turns over rapidly in G1 cells and interacts poorly with PALB2 in this phase of the cell cycle (Extended Data Fig. 10ab). However the most direct evidence that USP11 was under cell cycle regulation consists of the observation that there is a rapid loss of USP11 upon DNA damage induction, specifically in G1 phase (Fig 3e and Extended Data Fig. 10bc). The destabilization of USP11 following IR treatment is dependent on ATM signalling, whereas it is ATR-dependent following UV irradiation (Extended Data Fig. 10de). The drop in USP11 steady-state levels in G1 is the result of proteasomal degradation (Extended Data Fig. 10f). A CRL4 complex is most likely responsible for controlling the stability of USP11 as treatment with MLN492, a pan-CRL inhibitor²⁸ (Extended Data Fig. 10g), or depletion of CUL4 protected USP11 from DNA damage-induced degradation (Fig. 3f). CUL4 depletion led to BRCA2 and PALB2 IR-induced focus formation in G1 *53BP1Δ* cells (Fig. 3g and Extended Data Fig. 11), consistent with the regulation of USP11 by a CRL4 complex acting as the upstream signal that ultimately controls BRCA1-PALB2-BRCA2 complex assembly.

While deletion of 53BP1 produces low levels of ssDNA in G1 cells²⁹, combining the *53BP1Δ* mutation with depletion of KEAP1 did not produce extraction-resistant RAD51 IR-induced foci, suggesting little-to-no RAD51 nucleofilament formation. We surmised that ssDNA formation remained insufficient in those cells and thus took advantage of the phosphomimetic T847E mutant of CtIP that promotes resection in G1 cells³⁰. Unlike wild type CtIP, introduction of CtIP-T847E into *53BP1Δ* cells depleted of KEAP1 induced RAD51 IR-induced focus

formation in G1 cells (Fig 4ab and Extended Data Fig. 12ab) along with unscheduled DNA synthesis (Fig 4c). These results suggested that the steps downstream of RAD51 nucleofilament formation, i.e. strand invasion, D-loop formation and DNA synthesis, could be activated in G1.

To test whether productive HR could also be activated in G1 we employed a CRISPR/Cas9-stimulated gene targeting assay in which the insertion of the coding sequence for the mClover fluorescent protein at the 5' of the *LAMIN A* (*LMNA*) or *PML* genes was monitored by microscopy or flow cytometry (Fig 4d and Extended Data Fig. 12cd), with the latter method enabling the gating of cells with a defined DNA content (such as G1 cells). We also established synchronization protocols in which G1 cells obtained after release from a thymidine block were arrested in G1 by lovastatin treatment² for 24 h (Extended Data Fig. 12ef). With this system in hand, we first ascertained that gene targeting at the *LMNA* locus, was dependent on BRCA1-PALB2-BRCA2 complex assembly (Extended Data Fig. 13a), and that gene targeting by HR was highly suppressed in G1 (Fig 4e).

The combined activation of resection and BRCA1 recruitment to DSB sites (i.e. in *53BP1Δ* cells expressing CtIP-T847E) was insufficient to stimulate gene targeting at either the *LMNA* or the *PML* locus in G1 cells (Fig 4f and Extended Data Fig. 13bc). However, when the BRCA1-PALB2 interaction was restored in resection-competent G1 cells using either KEAP1 depletion or expression of the PALB2-KR mutant, we detected a robust increase in gene targeting events at both loci (Fig 4f and Extended Data Fig. 13bc). We note however that the gene-targeting frequencies of G1 cells remained lower than those of asynchronously dividing cells, suggesting an incomplete activation of HR. 53BP1 inactivation and the expression of CtIP-T847E were both necessary for G1 HR (Extended Data Fig. 14), indicating that the simultaneous activation of end resection and BRCA2 recruitment to DSB sites were both necessary and

sufficient to activate unscheduled recombination in this phase of the cell cycle.

We conclude that the regulation of BRCA1-PALB2-BRCA2 complex assembly is a key node in the cell cycle control of DSB repair by HR. This regulation converges on the BRCA1-interaction site on PALB2 and is enforced by the opposing activities of the E3 ligase CRL3-KEAP1 and the deubiquitylase USP11, with the latter being antagonized in G1 by a CRL4 complex (Fig. 4g). In this model, the stabilization of USP11 in S phase licenses the recruitment of PALB2-BRCA2 and the subsequent loading of RAD51 at DSB sites. Our studies also demonstrate that the suppression of HR in G1 cells is largely reversible and that it involves the combined suppression of end resection and BRCA2 recruitment to DSB sites. As most of the cells in the human body are in G0/G1 phase and thus refractory to gene targeting, the manipulations described herein may spur the development of genome editing methods that enable therapeutic gene targeting in a wider variety of tissues.

Acknowledgments

We are grateful to Rachel Szilard for critical reading of the manuscript, and also to Dara Lo, Marella Canny and Jordan Young for help with experiments on the project. We also thank Brett Larsen and Monika Tulcholska for technical support with the mass spectrometry, Jeremy Stark for the U2OS DR-GFP cells, Roger Greenberg for the U2OS 256 cells, Philip Reaper for the VE-821 inhibitor, Frank Sicheri for recombinant CDC34 and TEV protease, Feng Shao for the KEAP1 bacterial expression vector, David Cortez for the USP11 cDNA, Dimitris Xirodimas for the NEDD8 cDNA and Aude Echali er for the DEN1 cDNA. AO receives a post-doctoral fellowship from the CIHR; SMN receives a postdoctoral fellowship from the KWF; MDW holds a long-term HFSP fellowship; AS receives a graduate fellowship from OGS. JP was supported

by a trainee award from the Beatrice Hunter Cancer Research Institute (BHCRI) with funds provided by the Harvey Graham Cancer Research Fund as part of the Terry Fox Foundation Strategic Health Research Training Program in Cancer Research at CIHR. GD is a Senior Scientist of the BHCRI. DD is the Thomas Kierans Chair in Mechanisms of Cancer Development and a Canada Research Chair (Tier 1) in the Molecular Mechanisms of Genome Integrity. This work was supported by CIHR grants MOP89754 (to DD) and MOP84260 (to GD) and a Grant-in-Aid from the Krembil Foundation (to DD).

Author contributions

AO initiated the project and carried out most of the experiments. SMN carried out in vitro ubiquitylation experiments, pull-downs and mass spectrometry. MDW produced recombinant KEAP1 and advised on ubiquitylation biochemistry. SL produced the *53BP1A* cells. RIE produced active CUL3-RBX1. AS contributed to experiments on the regulation of USP11 degradation. MM helped AO on USP11 experiments. BX contributed critical PALB2 reagents and advice. JP and GD provided the vectors for the gene targeting assays. MP supervised RIE. DD supervised the project and wrote the manuscript with AO and with input from the other authors.

Correspondence and requests should be addressed to durocher@lunenfeld.ca

The authors declare no competing financial interests.

REFERENCES

- 1 Jasin, M. & Rothstein, R. Repair of strand breaks by homologous recombination. *Cold Spring Harb Perspect Biol* **5**, a012740, doi:10.1101/cshperspect.a012740 (2013).

- 2 Hartlerode, A., Odate, S., Shim, I., Brown, J. & Scully, R. Cell cycle-dependent induction of homologous recombination by a tightly regulated I-SceI fusion protein. *PLoS One* **6**, e16501, doi:10.1371/journal.pone.0016501 (2011).
- 3 Rothkamm, K., Kruger, I., Thompson, L. H. & Lobrich, M. Pathways of DNA double-strand break repair during the mammalian cell cycle. *Mol Cell Biol* **23**, 5706-5715 (2003).
- 4 Kasperek, T. R. & Humphrey, T. C. DNA double-strand break repair pathways, chromosomal rearrangements and cancer. *Semin Cell Dev Biol* **22**, 886-897, doi:10.1016/j.semcdb.2011.10.007 (2011).
- 5 Panier, S. & Durocher, D. Push back to respond better: regulatory inhibition of the DNA double-strand break response. *Nature reviews. Molecular cell biology*, doi:10.1038/nrm3659 (2013).
- 6 Ma, J. *et al.* PALB2 interacts with KEAP1 to promote NRF2 nuclear accumulation and function. *Mol Cell Biol* **32**, 1506-1517, doi:10.1128/MCB.06271-11 (2012).
- 7 Genschik, P., Sumara, I. & Lechner, E. The emerging family of CULLIN3-RING ubiquitin ligases (CRL3s): cellular functions and disease implications. *EMBO J* **32**, 2307-2320, doi:10.1038/emboj.2013.173 (2013).
- 8 Roy, R., Chun, J. & Powell, S. N. BRCA1 and BRCA2: different roles in a common pathway of genome protection. *Nat Rev Cancer* **12**, 68-78, doi:10.1038/nrc3181 nrc3181 [pii] (2011).
- 9 Li, M. L. & Greenberg, R. A. Links between genome integrity and BRCA1 tumor suppression. *Trends Biochem Sci*, doi:S0968-0004(12)00092-8 [pii] 10.1016/j.tibs.2012.06.007 (2012).
- 10 Park, J. Y., Zhang, F. & Andreassen, P. R. PALB2: The hub of a network of tumor suppressors involved in DNA damage responses. *Biochim Biophys Acta* **1846**, 263-275, doi:10.1016/j.bbcan.2014.06.003 (2014).
- 11 Schlegel, B. P., Jodelka, F. M. & Nunez, R. BRCA1 promotes induction of ssDNA by ionizing radiation. *Cancer Res* **66**, 5181-5189, doi:66/10/5181 [pii] 10.1158/0008-5472.CAN-05-3209 (2006).
- 12 Stark, J. M., Pierce, A. J., Oh, J., Pastink, A. & Jasin, M. Genetic steps of mammalian homologous repair with distinct mutagenic consequences. *Mol Cell Biol* **24**, 9305-9316, doi:24/21/9305 [pii] 10.1128/MCB.24.21.9305-9316.2004 (2004).
- 13 Zhang, F. *et al.* PALB2 links BRCA1 and BRCA2 in the DNA-damage response. *Curr Biol* **19**, 524-529, doi:S0960-9822(09)00723-4 [pii] 10.1016/j.cub.2009.02.018 (2009).
- 14 Sy, S. M., Huen, M. S. & Chen, J. PALB2 is an integral component of the BRCA complex required for homologous recombination repair. *P Natl Acad Sci USA* **106**, 7155-7160, doi:10.1073/pnas.0811159106 (2009).
- 15 Simhadri, S. *et al.* Male Fertility Defect Associated with Disrupted BRCA1-PALB2 Interaction in Mice. *J Biol Chem* **289**, 24617-24629, doi:10.1074/jbc.M114.566141 (2014).
- 16 Bhattacharyya, A., Ear, U. S., Koller, B. H., Weichselbaum, R. R. & Bishop, D. K. The breast cancer susceptibility gene BRCA1 is required for subnuclear assembly of Rad51 and survival following treatment with the DNA cross-linking agent cisplatin. *J Biol Chem* **275**, 23899-23903, doi:10.1074/jbc.C000276200

C000276200 [pii] (2000).

- 17 Zhang, F., Bick, G., Park, J. Y. & Andreassen, P. R. MDC1 and RNF8 function in a pathway that directs BRCA1-dependent localization of PALB2 required for homologous recombination. *J Cell Sci* **125**, 6049-6057, doi:10.1242/jcs.111872 (2012).
- 18 Escribano-Diaz, C. *et al.* A Cell Cycle-Dependent Regulatory Circuit Composed of 53BP1-RIF1 and BRCA1-CtIP Controls DNA Repair Pathway Choice. *Molecular cell* **49**, 872-883, doi:10.1016/j.molcel.2013.01.001 (2013).
- 19 Feng, L., Fong, K. W., Wang, J., Wang, W. & Chen, J. RIF1 counteracts BRCA1-mediated end resection during DNA repair. *The Journal of biological chemistry* **288**, 11135-11143, doi:10.1074/jbc.M113.457440 (2013).
- 20 Chapman, J. R. *et al.* RIF1 Is Essential for 53BP1-Dependent Nonhomologous End Joining and Suppression of DNA Double-Strand Break Resection. *Mol Cell*, doi:S1097-2765(13)00003-8 [pii] 10.1016/j.molcel.2013.01.002 (2013).
- 21 Bunting, S. F. *et al.* 53BP1 inhibits homologous recombination in Brca1-deficient cells by blocking resection of DNA breaks. *Cell* **141**, 243-254, doi:S0092-8674(10)00285-0 [pii] 10.1016/j.cell.2010.03.012 (2010).
- 22 Zimmermann, M., Lotterberger, F., Buonomo, S. B., Sfeir, A. & de Lange, T. 53BP1 Regulates DSB Repair Using Rif1 to Control 5' End Resection. *Science*, doi:science.1231573 [pii] 10.1126/science.1231573 (2013).
- 23 Tang, J. *et al.* Acetylation limits 53BP1 association with damaged chromatin to promote homologous recombination. *Nature structural & molecular biology*, doi:10.1038/nsmb.2499 (2013).
- 24 Taguchi, K., Motohashi, H. & Yamamoto, M. Molecular mechanisms of the Keap1-Nrf2 pathway in stress response and cancer evolution. *Genes Cells* **16**, 123-140, doi:10.1111/j.1365-2443.2010.01473.x (2011).
- 25 Sowa, M. E., Bennett, E. J., Gygi, S. P. & Harper, J. W. Defining the human deubiquitinating enzyme interaction landscape. *Cell* **138**, 389-403, doi:10.1016/j.cell.2009.04.042 (2009).
- 26 Schoenfeld, A. R., Apgar, S., Dolios, G., Wang, R. & Aaronson, S. A. BRCA2 is ubiquitinated in vivo and interacts with USP11, a deubiquitinating enzyme that exhibits prosurvival function in the cellular response to DNA damage. *Mol Cell Biol* **24**, 7444-7455, doi:10.1128/MCB.24.17.7444-7455.2004 24/17/7444 [pii] (2004).
- 27 Wiltshire, T. D. *et al.* Sensitivity to poly(ADP-ribose) polymerase (PARP) inhibition identifies ubiquitin-specific peptidase 11 (USP11) as a regulator of DNA double-strand break repair. *J Biol Chem* **285**, 14565-14571, doi:M110.104745 [pii] 10.1074/jbc.M110.104745 (2010).
- 28 Brownell, J. E. *et al.* Substrate-assisted inhibition of ubiquitin-like protein-activating enzymes: the NEDD8 E1 inhibitor MLN4924 forms a NEDD8-AMP mimetic in situ. *Mol Cell* **37**, 102-111, doi:10.1016/j.molcel.2009.12.024 (2010).
- 29 Yamane, A. *et al.* RPA accumulation during class switch recombination represents 5'-3' DNA-end resection during the S-G2/M phase of the cell cycle. *Cell Rep* **3**, 138-147, doi:10.1016/j.celrep.2012.12.006 (2013).

- 30 Huertas, P. & Jackson, S. P. Human CtIP mediates cell cycle control of DNA end resection and double strand break repair. *The Journal of biological chemistry* **284**, 9558-9565, doi:10.1074/jbc.M808906200 (2009).
- 31 Fradet-Turcotte, A. *et al.* 53BP1 is a reader of the DNA-damage-induced H2A Lys 15 ubiquitin mark. *Nature* **499**, 50-54, doi:10.1038/nature12318 (2013).
- 32 Enchev, R. I., Schreiber, A., Beuron, F. & Morris, E. P. Structural insights into the COP9 signalosome and its common architecture with the 26S proteasome lid and eIF3. *Structure* **18**, 518-527, doi:10.1016/j.str.2010.02.008 (2010).
- 33 Ran, F. A. *et al.* Genome engineering using the CRISPR-Cas9 system. *Nat. Protocols* **8**, 2281-2308, doi:10.1038/nprot.2013.143 (2013).
- 34 Xia, B. *et al.* Control of BRCA2 cellular and clinical functions by a nuclear partner, PALB2. *Mol Cell* **22**, 719-729, doi:10.1016/j.molcel.2006.05.022 (2006).
- 35 Orthwein, A. *et al.* Mitosis inhibits DNA double-strand break repair to guard against telomere fusions. *Science* **344**, 189-193, doi:10.1126/science.1248024 (2014).
- 36 Panier, S. *et al.* Tandem protein interaction modules organize the ubiquitin-dependent response to DNA double-strand breaks. *Molecular cell* **47**, 383-395, doi:10.1016/j.molcel.2012.05.045 (2012).
- 37 Juang, Y. C. *et al.* OTUB1 co-opts Lys48-linked ubiquitin recognition to suppress E2 enzyme function. *Mol Cell* **45**, 384-397, doi:10.1016/j.molcel.2012.01.011 S1097-2765(12)00077-9 [pii] (2012).
- 38 Cui, J. *et al.* Glutamine deamidation and dysfunction of ubiquitin/NEDD8 induced by a bacterial effector family. *Science* **329**, 1215-1218, doi:10.1126/science.1193844 (2010).
- 39 Enchev, R. I. *et al.* Structural basis for a reciprocal regulation between SCF and CSN. *Cell Rep* **2**, 616-627, doi:10.1016/j.celrep.2012.08.019 (2012).
- 40 Long, L., Furgason, M. & Yao, T. Generation of nonhydrolyzable ubiquitin-histone mimics. *Methods* **70**, 134-138, doi:10.1016/j.ymeth.2014.07.006 (2014).

FIGURE LEGENDS

Figure 1. Inhibition of the BRCA1-PALB2 interaction in G1 is CRL3-KEAP1-dependent.

a, U2OS cells synchronized in G1 after release from a double-thymidine block were irradiated (2 Gy) and processed for γ -H2AX, BRCA1 and BRCA2 immunofluorescence. **b**, Quantitation of the experiment shown in **a** and [Extended Data Fig. 1d](#). ASN=asynchronously dividing cells. WT, wild type (mean \pm s.d., $N=3$). **c**, Immunoprecipitation (IP) of endogenous PALB2 from extracts prepared from mock- or X-irradiated 293T cells synchronized in S or G1 phases. IP with normal IgG was performed as a control. Cyclin A (CCNA) immunoblotting demonstrates the efficacy of the synchronization. **d**, Quantitation of the experiment shown in [Extended Data Fig. 3a](#).

53BP1 Δ U2OS cells were transfected with the indicated GFP-PALB2 vectors and siRNAs and irradiated (20 Gy) before being processed for fluorescence microscopy. Cells were also stained with a Cyclin A (CCNA) antibody to determine cell cycle position (mean \pm s.d., $N=3$). **e**, IP of PALB2 from extracts prepared from synchronized and irradiated 293T cells of the indicated genotypes. IP with normal IgG was performed as a control. **f**, 293T cells with the indicated genotypes were transfected with the indicated HA-KEAP1 constructs, synchronized in G1 or S phases and irradiated. Cells were processed for PALB2 immunoprecipitation (IP). EV, empty vector.

Figure 2. Ubiquitylation of PALB2 prevents BRCA1-PALB2 interaction.

a, Sequence of the N-terminal region of PALB2 and the different mutants used. **b**, 293T cells were transfected with the indicated GFP-PALB2 constructs and synchronized in G1 or S phase. Cells were processed for GFP immunoprecipitation (IP). **c**, Schematic of the *LacO/LacR* chromatin-targeting system

and the *in vivo* quantification of ubiquitylated PALB2. **d**, U2OS 256 cells were transfected with the indicated mCherry-LacR-PALB2 vectors. Cells were processed for quantitation of FK2 fluorescence at the mCherry focus. Each circle represents a cell analyzed from 3 independent experiments and the bar is at the median. Cells were also stained with a Cyclin A antibody to determine cell cycle position. *** denotes $P < 0.001$ between the G1 and S/G2 conditions calculated with a one-way ANOVA with Bonferroni correction. **e**, *In vitro* ubiquitylation of the indicated HA-tagged PALB2 protein by KEAP1 and the NEDDylated CUL3/RBX1 complex. CDC34 was used as the E2 conjugating enzyme. **f**, Pulldown assay of *in vitro* ubiquitylated HA-PALB2 (1-103) incubated with MBP or MBP-BRCA1-CC. I: input, PD: pulldown, FT: flow-through.

Figure 3. USP11 opposes the activity of CRL3-KEAP1. **a**, 293T cells with the indicated genotypes were transfected with the indicated GFP-USP11 constructs and treated with CPT. Cells were processed for normal IgG control or PALB2 immunoprecipitation. CS, C318S. **b**, Clonogenic survival assays of 293T cells of the indicated genotypes in the presence of olaparib (mean \pm s.d., $N=4$). **c**, 293T cells of the indicated genotypes were treated with CPT and then processed for normal IgG or PALB2 immunoprecipitation (IP). **d**, HA-tagged PALB2 (1-103) was ubiquitylated *in vitro* with lysine-less Ub, and then subjected to deubiquitylation using increasing concentrations of GST-USP11 or its catalytically-inactive mutant (CS). USP2 was used as a control. **e**, U2OS cells synchronized in the indicated cell cycle phases were irradiated with a 20 Gy dose, harvested at the indicated time points and processed for USP11 and actin immunoblotting. **f**, U2OS cells were transfected with the indicated siRNAs, irradiated and processed for immunoblotting. **g**, *53BP1Δ* U2OS cells were transfected with the indicated

siRNA, synchronized in G1 by release from a double-thymidine block, and irradiated (20 Gy) before being processed for fluorescence microscopy. The percentage of cells with more than 5 γ -H2AX-colocalizing BRCA2 foci is indicated (mean \pm s.d., $N=3$).

Figure 4. Reactivation of HR in G1 phase. **a**, Quantification of wild type (WT) and *53BP1 Δ* U2OS cells co-transfected with non-targeting (CTRL) or KEAP1 siRNAs and vectors expressing WT CtIP or the T847E (TE) mutant that cells were synchronized in G1, irradiated (2 Gy) and processed for γ -H2AX and RAD51 immunofluorescence (mean \pm s.d., $N=3$). **b**, Representative micrograph from the quantification shown in **a**. **c**, U2OS *53BP1 Δ* cells were synchronized in G1, supplemented with BrdU, irradiated (2 Gy) and processed for γ -H2AX and BrdU immunofluorescence. The percentage of cells with more than 5 γ -H2AX-colocalizing BrdU foci is indicated (mean \pm s.d., $N=3$). **d**, Schematic of the assay in which the open reading frame of mClover is inserted at the 5' end of the coding sequence of the *LMNA* (or *PML*) gene following a CRISPR/Cas9-mediated DSB. **e**, Quantitation of gene targeting efficiency at the *LMNA* locus in asynchronously dividing (ASN) and G1-arrested U2OS cells. Gene targeting events were detected by flow cytometry (mean \pm s.d., $N=3$). **f**, Gene targeting efficiency at the *LMNA* locus measured by flow cytometry in G1-arrested cells transfected with the indicated siRNA or a PALB2-KR expression vector (mean \pm s.d., $N=3$). **g**, Model of the cell-cycle regulated assembly of the BRCA1-PALB2-BRCA2 complex.

EXTENDED DATA FIGURE LEGENDS

Extended Data Figure 1 | Related to Fig. 1. a, Schematic representation of human 53BP1 gene organization and targeting sites of sgRNAs used. Boxes indicate exons (E: yellow, coding sequence; brown, untranslated regions (UTRs)). The indels introduced by CRISPR/Cas9 and their respective frequencies are indicated. **b**, Wild-type (WT) and *53BP1Δ* and U2OS cells were mock- or X-irradiated (10 Gy) before being processed for 53BP1 fluorescence microscopy. DAPI was used to stain DNA and trace the outline of the nucleus. **c**, Wild-type (WT) and *53BP1Δ* U2OS cells were processed for 53BP1 immunoblotting. Tubulin was used as a loading control. **d**, Wild-type (WT) and *53BP1Δ* U2OS cells either synchronized in G1 following a double-thymidine block and release or asynchronously dividing (ASN), were irradiated (2 Gy) and processed for γ -H2AX, PALB2, BRCA2 and BRCA1, immunofluorescence. The micrographs relating to BRCA1 and BRCA2 staining in G1 are found in Fig. 1a. **e**, Wild-type (WT) and *53BP1Δ* U2OS cells synchronized in G1 after release from a double-thymidine block were irradiated (20 Gy) and processed for γ -H2AX, BRCA1 and BRCA2 immunofluorescence. On the left are representative micrographs for the G1-arrested cells and the quantitation of the full experiment is shown on the right (mean \pm s.d., $N=3$).

Extended Data Figure 2 | Related to Fig. 1. a, Schematic of the *LacO*/LacR chromatin-targeting system. **b**, U2OS 256 cells were transfected with the indicated mCherry-LacR and GFP-fusions. GFP fluorescence was measured at the site of the *LacO* array-localized mCherry focus. Each circle represents one cell analysed and the bar is at the median. Cells were also

stained with a Cyclin A antibody to determine cell cycle position ($N=3$). **c**, Representative micrographs of U2OS 256 cells transfected with the indicated mCherry-LacR and GFP-fusions; data is quantified in **d**. **d**, Quantification of U2OS 256 cells transfected with the indicated mCherry-LacR and GFP-fusion to tether either BRCA1 or PALB2 to the *LacO* array. BRCA1-CC: coiled-coil domain interacting with PALB2 ($N=3$). **e**, Schematic representation of PALB2 architecture and its major interacting proteins. **f**, Quantification of U2OS 256 cells transfected with the indicated GFP-PALB2 mutants and mCherry-LacR-BRCA1-CC. Cells were also stained with a Cyclin A antibody to determine cell cycle position ($N=3$).

Extended Data Figure 3 | Related to Fig. 1 and 2. **a**, Representative micrographs of the experiment shown in Fig. 1d. **b**, Schematic representation of human *KEAP1* gene organization and targeting sites of sgRNAs used as described in Extended Data Fig.1. **a**. The indels introduced by CRISPR/Cas9 and their respective frequencies are indicated. **c**, Immunoprecipitation (IP) of PALB2 from extracts prepared from irradiated 293T cells. IP with normal IgG was performed as a control. **d**, Quantification of U2OS 256 cells transfected with the indicated GFP-PALB2 mutants and mCherry-LacR-BRCA1. Cells were also stained with a Cyclin A antibody to determine cell cycle position ($N=3$). **e**, Quantification of U2OS 256 cells transfected with GFP-PALB2 and the indicated mCherry-LacR-BRCA1-CC (CC: coiled-coil) mutants. Cells were also stained with a Cyclin A antibody to determine cell cycle position ($N=3$). This panel shows that the sole lysine in the PALB2-interaction motif is not involved in the cell cycle regulation of the PALB2-BRCA1 interaction.

Extended Data Figure 4 | Related to Fig. 2. **a**, HEK293 Flp-In T-REX cells expressing doxycycline (DOX)-inducible His₆-Ub were transfected with the indicated siRNAs. Cells were processed for Ni-NTA pull-down (IP). **b**, 293T cells transfected with an siRNA targeting USP11 and a Flag-PALB2 expression vector were processed for Flag immunoprecipitation followed by mass spectrometry. Representative MS2 spectra of tryptic diglycine (diG)-PALB2 peptides identified and shown (K16, top; K43, bottom). **c**, Representative micrographs of the experiment shown in Fig. 2d. Scale bar = 5 μ m.

Extended Data Figure 5 | Related to Fig. 2. HA-PALB2 (1-103) was subjected to *in vitro* ubiquitylation reactions that lacked (left panels) or included (right panels) CUL3. Representative fragmentation spectra of tryptic peptides from the reaction products are shown. For each peptide, the traces from top to bottom show: total ion current; basepeak chromatograms of the heavy- and light-labeled peptide mass, respectively; representative MS/MS fragmentation spectra of the heavy- and light-labeled peptide, respectively. The heavy-labeled amino acid is indicated by an asterisk (*).

Extended Data Figure 6 | Related to Fig. 2. Site-specific chemical ubiquitylation of PALB2 (1-103) at residue 20 (PALB2-K_C20-Ub) and 45 (PALB2-K_C45-Ub) was carried out by dichloroacetone linking. The resulting ubiquitylated PALB2 polypeptides along with their unmodified counterparts were subjected to pulldown with a fusion of MBP with the coiled-coil domain of BRCA1 (MBP-BRCA1-CC). I, input; PD, pulldown. Asterisk (*) indicates a non-specific band.

Extended Data Figure 7 | Related to Fig. 3. a, Wild-type and *KEAP1Δ* 293T cells were treated with cycloheximide (CHX) for the indicated time and then processed for NRF2 and KEAP1 immunoblotting. Actin levels were also determined as a loading control.

Extended Data Figure 8 | Related to Fig. 3. a, Immunoprecipitation (IP) of USP11 from extracts prepared from 293T cells that were or were not treated with camptothecin (CPT; 200 nM). IP with normal IgG was performed as a control. **b,** U2OS DR-GFP cells were transfected with the indicated siRNAs. 24 h post-transfection, cells were further transfected with the indicated siRNA-resistant USP11 expression vectors (WT=wild type; CA= C318A and CS= C318S catalytically-dead mutants) or an empty vector (EV), with or without an I-SceI expression vector. The percentage of GFP-positive cells was determined 48 h post-plasmid transfection for each condition and was normalized to the I-SceI + non-targeting (siCTRL) condition (mean ± s.d., *N*=3). **c,** Schematic representation of human *USP11* (top) and *KEAP1* (bottom) gene organization and targeting sites of sgRNAs (as described in Extended Data Figure 1a) used to generate the *USP11Δ* and *USP11Δ/KEAP1Δ* 293T cells. The indels introduced by the CRISPR/Cas9 and their respective frequencies are indicated. The USP11 knockout was created first and subsequently used to make the *USP11Δ/KEAP1Δ* double mutant. **d,** Immunoprecipitation (IP) of PALB2 from extracts prepared from 293T cells transfected with the indicated siRNA and with or without CPT (200 nM) treatment. IP with normal IgG was performed as a control.

Extended Data Figure 9 | Related to Fig. 3. a, U2OS DR-GFP cells were transfected with the indicated siRNAs or left untransfected (-). 24 h post-transfection, cells were transfected with an

I-SceI expression vector (circle). The percentage of GFP-positive cells was determined 48 h post-plasmid transfection for each condition and was normalized to the I-SceI + non-targeting (CTRL) condition (mean \pm s.d., $N=3$). **b**, Parental 293T cells or a *USP11Δ* derivative were transfected with the indicated GFP-PALB2 constructs, treated with CPT and processed for GFP immunoprecipitation (IP). **c**, Parental 293T cells (WT) or a *USP11Δ* derivative were transfected with an empty vector (EV) or the indicated PALB2 expression vectors. Sensitivity of the cells to the PARP inhibitor Olaparib was then determined by a clonogenic survival assay (mean \pm s.d., $N=3$).

Extended Data Figure 10 | Related to Fig. 3. **a**, U2OS cells synchronized in G1 or S/G2 were treated with cyclohexamide (CHX) and processed at the indicated time points to monitor USP11 stability. **b**, Immunoprecipitation (IP) of PALB2 from extracts prepared from 293T cells that were synchronized in G1 or S phase and treated or not with IR (20 Gy). **c**, U2OS cells were irradiated with a dose of 2 or 20 Gy and processed for USP11 immunoblotting at the indicated times post-IR. Actin was used as a loading control. **d**, U2OS cells, mock-treated or incubated with the ATM (KU55933; ATMi), ATR (VE-821; ATRi) or DNA-PKcs (NU7441; DNAPKi) inhibitors, were irradiated (20 Gy) and processed for USP11 and actin (loading control) immunoblotting. **e**, Similar experiment to **d** except that cells were UV-irradiated with a 50 mJ/cm² dose. **f**, U2OS cells, mock-treated or incubated with the proteasome inhibitor MG132, were irradiated (20 Gy) and processed for USP11 and actin (loading control) immunoblotting. **g**, U2OS cells, mock-treated or incubated with the Cullin inhibitor MLN4924, were irradiated (20 Gy) and processed for USP11 and actin (loading control) immunoblotting.

Extended Data Figure 11 | Related to Fig. 3. *53BP1Δ* U2OS cells were transfected with the indicated siRNA, synchronized in G1 or S/G2 by release from a double-thymidine block and irradiated (20 Gy) before being processed for fluorescence microscopy. DAPI was used to trace the nuclear boundary and Cyclin A staining was used to determine cell cycle position. The percentage of cells with more than 5 γ -H2AX-colocalizing PALB2 foci is indicated as the mean \pm s.d., $N=3$. Scale bar = 5 μ m.

Extended Data Figure 12 | Related to Fig. 4. **a**, Representative micrographs of irradiated G1-synchronized wild-type (WT) and *53BP1Δ* U2OS cells transfected with the indicated siRNA and expressing wild-type (WT) CtIP. **b**, Representative micrographs of irradiated G1-synchronized *53BP1Δ*U2OS cells transfected with the indicated siRNA and expressing CtIP-T847E. **c**, Micrograph of a U2OS cell targeted with the mClover system showing the typical perinuclear expression pattern of Lamin A. **d**, Micrograph of a U2OS cell targeted with the mClover system showing an expression pattern characteristic of subnuclear PML foci. **e**, Timeline of the gene targeting (*LMNA*) experiment presented in Fig 4e. **f**, Timeline of the gene targeting (*LMNA* or *PML*) experiment presented in Fig 4f and Extended Data Figure 13.

Extended Data Figure 13 | Related to Fig. 4. **a**, Quantitation of gene targeting efficiency at the *LMNA* locus in asynchronously dividing cells transfected with the indicated siRNA. Gene targeting events were detected by flow cytometry (mean \pm s.d., $N=3$). **b**, Gene targeting efficiency at the *PML* locus measured by flow cytometry in G1-arrested *53BP1Δ* U2OS cells expressing the CtIP-T847E mutant and co-transfected with the indicated siRNA or a PALB2-KR expression construct (mean \pm s.d., $N=3$). **c**, Representative FACS profiles showing the gating for

1N DNA content cells and the detection of mClover-positive cells in the *LMNA* gene targeting assay in asynchronous (ASN) or G1-arrested *53BP1Δ* U2OS cells expressing the CtIP-T847E mutant and co-transfected with the indicated siRNA or a PALB2-KR expression construct.

Extended Data Figure 14 | Related to Fig. 4. a, Gene targeting efficiency at the *LMNA* locus measured by flow cytometry in G1-arrested parental (WT) and *53BP1Δ* U2OS cells transfected with KEAP1 siRNA and expressing the CtIP-T847E mutant (mean \pm s.d., $N=3$). **b,** Gene targeting efficiency at the *LMNA* locus measured by flow cytometry in G1-arrested parental (WT) and *53BP1Δ* U2OS cells transfected with the indicated siRNA and expressing either wild-type (WT) or the CtIP-T847E mutant (mean \pm s.d., $N=3$).

METHODS

Plasmids

The cDNA of PALB2 was obtained from the Mammalian Gene Collection (MGC). Full length PALB2 and BRCA1 were amplified by PCR, subcloned into pDONR221 and delivered into the pDEST-GFP, pDEST-Flag and the mCherry-LacR vectors using Gateway cloning technology (Invitrogen). Similarly, the coiled-coil domain of BRCA1 was amplified by PCR, subcloned into the pDONR221 vector and delivered into both mCherryLacR and pDEST-GFP vectors. The N-terminal domain of PALB2 was amplified by PCR and introduced into the GST expression vector pET30-2-His-GST-TEV³¹ using the EcoRI/XhoI sites. The coiled-coil domain of BRCA1 was cloned into pMAL-c2 using the BamHI/SalI sites. Truncated forms of PALB2 were obtained by introducing stop codons or deletions through site-directed mutagenesis. Full-length CtIP was amplified by PCR, subcloned into the pDONR221 and delivered into the lentiviral construct pCW57.1 (a kind gift of Dr. David Root; Addgene plasmid #41393) using Gateway cloning technology (Invitrogen). The USP11 cDNA was a kind gift of David Cortez and was amplified by PCR and cloned into the pDsRed2-C1 vector using the EcoRI/SalI sites. The bacterial codon-optimised coding sequence of pig USP11 (USP11) was subcloned into the 6xHis-GST vector pETM-30-Htb using the BamHI/EcoRI sites. siRNA-resistant versions of PALB2, BRCA1 and USP11 constructs were generated as previously described (11). Full-length CUL3 and RBX1 were amplified by PCR from a human pancreas cDNA library (Invitrogen) as previously described³² and cloned into the dual expression pFBDM vector using NheI/XmaI and BssHII/NotI respectively. The NEDD8 cDNA was a kind gift of Dmitris Xirodimas and was fused to a double StrepII tag at its C-terminus in the pET17b vector (Millipore). Human DEN1

was amplified from a vector supplied by Aude Echali er and fused to a non-cleavable N-terminal StrepII2x tag by PCR and inserted into a pET17b vector. The pCOOL-mKEAP1 plasmid was a kind gift from Dr. Feng Shao. The pcDNA3-HA2-KEAP1 and pcDNA3-HA2-KEAP1 BTB were kind gifts from Dr. Yue Xiong (Addgene plasmids #21556 and 21593). gRNAs were synthesized and processed as described previously³³. Annealed gRNAs were cloned into the Cas9-expressing vectors pSpCas9(BB)-2A-Puro (PX459) or pX330-U6-Chimeric_BB-CBh-hSpCas9, a kind gift from Feng Zhang (Addgene plasmids #48139 and 42230). The gRNAs targeting the *LMNA* or the *PML* locus and the mClover-tagged *LMNA* or *PML* are from Pinder et al (*submitted*). The lentiviral packaging vector psPAX2 and the envelope vector VSV-G were a kind gift from Didier Trono (Addgene plasmids #12260 and 12259). 6xHis-Ubiquitin was cloned into the pcDNA5-FRT/TO backbone using the XhoI/HindIII sites. All mutations were introduced by site-directed mutagenesis using QuikChange (Stratagene) and all plasmids were sequence-verified.

Cell culture and plasmid transfection

All culture media were supplemented with 10% fetal bovine serum (FBS). U-2-OS (U2OS) cells were cultured in McCoy's medium (Gibco). 293T cells were cultured in DMEM (Gibco). Parental cells were tested for mycoplasma contamination and authenticated by STR DNA profiling. Plasmid transfections were carried out using Lipofectamine 2000 Transfection Reagent (Invitrogen) following the manufacturer's protocol. Lentiviral infection was carried out as previously described¹⁸.

Antibodies

We employed the following antibodies: rabbit anti-53BP1 (A300-273A, Bethyl), rabbit anti-53BP1 (sc-22760, Santa Cruz), mouse anti-53BP1 (#612523, BD Biosciences), mouse anti- γ -H2AX (clone JBW301, Millipore), rabbit anti- γ -H2AX (#2577, Cell Signaling Technologies), rabbit anti-KEAP1 (ab66620, Abcam), rabbit anti-NRF2 (ab62352, Abcam), mouse anti-Flag (clone M2, Sigma), mouse anti-tubulin (CP06, Calbiochem), mouse anti-GFP (#11814460001, Roche), mouse anti-CCNA (MONX10262, Monosan), rabbit anti-BRCA2 (ab9143, Abcam), mouse anti-BRCA2 (OP95, Calbiochem), rabbit anti-BRCA1 (#07-434, Millipore), rabbit anti-USP11 (ab109232, Abcam), rabbit anti-USP11 (A301-613A, Bethyl), rabbit anti-RAD51 (#70-001, Bioacademia), mouse anti-BrdU (RPN202, GE Healthcare), mouse anti-FK2 (BML-PW8810, Enzo), rabbit anti-PALB2³⁴, rabbit anti-GST (sc-459, Santa Cruz), rabbit anti-CUL3 (A301-108A, Bethyl), mouse anti-MBP (E8032, NEB), mouse anti-HA (clone 12CA5, a kind gift of Dr. M. Tyers), rabbit anti-Ubiquitin (Z0458, Dako) and mouse anti-actin (CP01, Calbiochem). The following antibodies were used as secondary antibodies in immunofluorescence microscopy: Alexa Fluor 488 donkey anti-rabbit IgG, Alexa Fluor 488 donkey anti-goat IgG, Alexa Fluor 555 donkey anti-mouse IgG, Alexa Fluor 555 donkey anti-rabbit IgG, Alexa Fluor 647 donkey anti-mouse IgG, Alexa Fluor 647 donkey anti-human IgG, Alexa Fluor 647 donkey anti-goat IgG (Molecular Probes).

RNA interference

All siRNAs employed in this study were single duplex siRNAs purchased from ThermoFisher. RNAi transfections were performed using Lipofectamine RNAiMax (Invitrogen) in a forward transfection mode. The individual siRNA duplexes used were: BRCA1 (D-003461-05), PALB2 (D-012928-04), USP11 (D-006063-01), CUL1 (M-004086-01), CUL2 (M-007277-00), CUL3

(M-010224-02), CUL4A (M-012610-01), CUL4B (M-017965-01), CUL5 (M-019553-01), KEAP1 (D-12453-02), RAD51 (M-003530-04), CtIP/RBBP8 (M-001376-00), BRCA2 (D-003462-04), 53BP1 (D-003549-01) and non-targeting control siRNA (D-001210-02). Except when stated otherwise, siRNAs were transfected 48 h prior to cell processing.

Inhibitors and fine chemicals

We employed the following drugs at the indicated concentration and time: cycloheximide (CHX; Sigma) at 100 ng/mL, camptothecin (CPT; Sigma) at 0.2 μ M, ATM inhibitor (KU55933; Selleck Chemicals) at 10 μ M, ATR inhibitor (VE-821; kind gift of Philip Reaper) at 10 μ M, DNA-PKcs inhibitor (NU7441; Genetex) at 10 μ M, proteasome inhibitor MG132 (Sigma) at 2 μ M, Lovastatin (S2061; Selleck Chemicals) at 40 μ M, Doxycycline (#8634-1; Clontech), Nedd8-activating enzyme inhibitor (MLN4929; Active Biochem) at 5 μ M and olaparib (Selleck) at the indicated concentrations.

Immunofluorescence microscopy

In most cases, cells were grown on glass coverslips, fixed with 2% (w/v) paraformaldehyde in PBS for 20 min at room temperature, permeabilized with 0.3 % (v/v) Triton X-100 for 20 min at room temperature and blocked with 5% BSA in PBS for 30 min at room temperature. Alternatively, cells were fixed with 100% cold methanol for 10 min at -20°C and subsequently washed with PBS for 5 min at room temperature before PBS-BSA blocking. Cells were then incubated with the primary antibody diluted in PBS-BSA for 2 h at room temperature. Cells were next washed with PBS and then incubated with secondary antibodies diluted in PBS-BSA supplemented with 0.8 μ g/ml of DAPI to stain DNA for 1 h at room temperature. The coverslips

were mounted onto glass slides with Prolong Gold mounting agent (Invitrogen). Confocal images were taken using a Zeiss LSM780 laser-scanning microscope. For G1 vs. S/G2 analysis of the BRCA1-PALB2-BRCA2 axis, cells were first synchronized with a double-thymidine block, released to allow entry into S phase and exposed to 2 or 20 Gy of X-irradiation at 5h and 12h post-release and fixed at 1 to 5 hours post-treatment (where indicated). For the examination of DNA replication, cells were pre-incubated with 30 μ M BrdU for 30 min before irradiation and processed as previously described.

CRISPR/Cas9 genome editing of USP11/KEAP1

293T and U2OS cells were transiently transfected with 3 distinct sgRNAs targeting either 53BP1, USP11 or KEAP1 and expressed from the pX459 vector containing Cas9 followed by the 2A-Puromycin cassette. The next day, cells were selected with puromycin for 2 days and subcloned to form single colonies or subpopulations. Clones were screened by immunoblot and/or immunofluorescence to verify the loss of 53BP1, USP11 or KEAP1 expression and subsequently characterized by PCR and sequencing. The genomic region targeted by the CRISPR/Cas9 was amplified by PCR using Turbo Pfu polymerase (Agilent) and the PCR product was cloned into the pCR2.1 TOPO vector (Invitrogen) before sequencing.

Olaparib clonogenic assay

293T cells were incubated with the indicated doses of olaparib (Selleck Chemicals) for 24 h, washed once with PBS and counted by trypan blue staining. 500 cells were then plated in duplicate for each condition. The cell survival assay was performed as previously described³⁵.

Recombinant protein production

GST and MBP fusion proteins were produced as previously described^{36,37}. Briefly, MBP proteins expressed in *Escherichia coli* were purified on amylose resin (New England Biolabs) according to the batch method described by the manufacturer and stored in 1X PBS, 5% glycerol. GST proteins expressed in *E. coli* were purified on glutathione sepharose 4B (GE Healthcare) resin in 50 mM Tris HCl pH 7.5, 300 mM NaCl, 2 mM DTT, 1 mM EDTA, 15 µg/mL AEBSF and 1x Complete protease inhibitor cocktail (Roche). Upon elution from the resin using 50 mM glutathione in 50 mM Tris HCl pH 8, 2 mM DTT, the His₆-GST tag was cleaved off using His-tagged TEV protease (kindly provided by F. Sicheri) in 50 mM Tris HCl pH 7.5, 150 mM NaCl, 10 mM glutathione, 10% glycerol, 2 mM sodium citrate and 2 mM β-mercaptoethanol. His₆-tagged proteins were depleted using Ni-NTA-agarose beads (Qiagen) in 50 mM Tris HCl pH 7.5, 300 mM NaCl, 20 mM imidazole, 5 mM glutathione, 10% glycerol, 1 mM sodium citrate and 2 mM β-mercaptoethanol followed by centrifugal concentration (Amicon centrifugal filters, Millipore). GST-mKEAP1 was purified as described previously³⁸, with an additional anion exchange step on a HiTrap Q HP column (GE Healthcare). The GST tag was left on the protein for *in vitro* experiments. Purification of CUL3 and RBX1 was performed as previously described³². Nedd8 and Den1 were expressed in *E. coli* BL21 grown in Terrific broth media and induced overnight with 0.5 mM IPTG at 16°C. Cells were harvested and resuspended in wash buffer (400 mM NaCl, 50 mM Tris-HCl, pH 8, 5% glycerol, 2 mM DTT), supplemented with lysozyme, universal nuclease (Pierce), benzamidine, leupeptin, pepstatin, PMSF and Complete protease inhibitor cocktail (Roche), except for Dcn1-expressing cells where the protease inhibitors were omitted. Cells were lysed by sonication and the lysate was cleared by centrifugation at 20,000 rpm for 50 min. The soluble supernatant was bound to a 5 ml Strep-

Tactin Superflow Cartridge with a flow rate of 3 ml/min using a peristaltic pump. The column was washed with 20 column volumes (CV) of washing buffer and eluted with 5 CV washing buffer, diluted 1:2 in water to reduce the final salt concentration, and supplemented with 2.5 mM desthiobiotin. The elution fractions were pooled and concentrated to a total volume of 4 ml using a 3 kDa cut-off Amicon concentrator. Den1 was further purified over a Superdex 75 size exclusion column, buffer exchanged into 150 mM NaCl, HEPES, pH 7.6, 2 % glycerol and 1 mM DTT. The C-terminal pro-peptide and StrepII2x-tag were removed by incubation with StrepII2x-Dcn1 in 1:20 molar ratio for 1 hour at room temperature. The Den1 cleavage reaction was buffer exchanged on a Zeba MWCO desalting column (Pierce), to remove the desthiobiotin, and passed through a Strep-Tactin Cartridge, which retains the C-terminal pro-peptide and Den1. GST-USP11 proteins were expressed in *E. coli* as described {Hendriks, 2015 #6222}. Cells were lysed by lysozyme treatment and sonication in 50mM Tris pH 7.5, 300mM NaCl, 1mM EDTA, 1mM AEBSF, 1 x Protease Inhibitor mix (284 ng/ml leupeptin, 1.37 µg/ml pepstatin A, 170 µg/ml PMSF and 330 µg/ml benzamidine) and 5% glycerol. Cleared lysate was applied to a column packed with glutathione sepharose 4B (GE Healthcare), washed extensively with lysis buffer before elution in 50mM Tris pH 7.5, 150mM NaCl, 5% glycerol and 25mM reduced glutathione. DUB activity was assayed on fluorogenic Ubiquitin-AMC, measured using a Synergy Neo microplate reader (Biotek).

***In vitro* ubiquitylation and deubiquitylation of PALB2**

HA-tagged N-terminal fragments of PALB2 (1-103) (1 µM) were *in vitro* ubiquitylated using 50 µM wild-type (Ubi WT, Boston Biochem) or a lysine-less ubiquitin (Ubi K0, Boston Biochem), 100 nM human Uba1 (E1), 500 nM CDC34 (kindly provided by F. Sicheri and D. Ceccarelli),

250 nM neddylated CUL3/RBX1, 375 nM GST-mKEAP1 and 1.5 mM ATP in a buffer containing 50 mM Tris HCl pH 7.5, 20 mM NaCl, 10 mM MgCl₂ and 0.5 mM DTT. Ubiquitylation reactions were carried out at 37 °C for 1 hour, unless stated otherwise. For USP11-mediated deubiquitylation assays, HA-PALB2 (1-103) was first ubiquitylated using lysine-less ubiquitin with enzyme concentrations as described above in 50 µL reactions in a buffer containing 25mM HEPES pH 8, 150 mM NaCl, 10 mM MgCl₂, 0.5 mM DTT and 1.5 mM ATP for 1.5 h at 37 °C. Reactions were stopped by the addition of 1 unit Apyrase (New England Biolabs). Reaction products were mixed at a 1:1 ratio with wild-type or catalytically inactive (C270S) USP11, or USP2 (kindly provided by Dr. F. Sicheri and E. Zeqiraj) using final concentrations of 100 nM – 500 nM – 2500 nM (USP11) and 500 nM (USP2) and incubated for 2 h at 30 °C in a buffer containing 25 mM Hepes pH 8, 150 mM NaCl, 2 mM DTT, 0.1 mg/mL BSA, 0.03% Brij-35, 5 mM MgCl₂, 0.375 mM ATP.

Pulldown experiments between purified PALB2 and BRCA1

PALB2 *in vitro* ubiquitylation reaction products were diluted in a buffer at final concentration of 50 mM Tris-HCl pH 7.5, 150 mM NaCl, 5 mM MgCl₂, 0.25 mM DTT and 0.1% NP-40. 20 µg MBP or MBP-BRCA1-CC (coiled coil region of BRCA1) was coupled to amylose resin (New England Biolabs) in the above buffer supplemented with 0.1% BSA prior to addition of the ubiquitylation products. Pulldown reactions were performed at 4 °C for 2 h, followed by extensive washing.

Co-immunoprecipitation

Cells were collected by trypsinization, washed once with PBS and lysed in 500 µL of lysis buffer

(20 mM Tris-HCl pH 8.0, 150 mM NaCl, 10% glycerol, 2 mM EDTA, 1% NP-40, Complete protease inhibitor cocktail (Roche), cocktail of phosphatase inhibitors (Sigma) and N-ethylmaleimide to inhibit deubiquitination) on ice. Lysates were centrifuged at 15 000 g for 10 min at 4°C and protein concentration was evaluated using absorbance at 280 nm. Equivalent amounts of proteins (~0.5-1 mg) were incubated with 2 µg of rabbit anti-PALB2, rabbit anti-USP11 antibody, rabbit anti-GFP antibody or normal rabbit IgG for 5 h at 4°C. A mix of protein A/protein G-Sepharose beads (Thermo Scientific) was added for an additional hour. Beads were collected by centrifugation, washed twice with lysis buffer and once with PBS, and eluted by boiling in 2X Laemmli buffer before analysis by SDS-PAGE and immunoblotting.

Mass spectrometry

Following immunoprecipitation of transiently transfected Flag-PALB2 from siCTRL-transfected or USP11 siRNA-depleted 293T cells, cysteine residues were reduced and alkylated using DTT and 2-chloroacetamide, respectively. Proteins were digested using limited trypsin digestion on beads (1 µg trypsin (Worthington, NJ, USA) per sample, 20 min at 37°C), and dried to completeness. For LC-MS/MS analysis, peptides were reconstituted in 5% formic acid and loaded onto a 12-15 cm fused silica column with pulled tip packed in-house with 3.5 µm Zorbax C18 (Agilent Technologies, CA, USA). Samples were analyzed using an Orbitrap Velos (Thermo Scientific, MA, USA) coupled to an Eksigent nanoLC ultra (AB SCIEX, CA). Peptides were eluted from the column using a 90 min period cycle with a linear gradient from 2% to 35% acetonitrile in 0.1% formic acid. Tandem MS spectra were acquired in a data-dependent mode for the top two most abundant and five most specific N-terminal PALB2 tryptic digest peptides, either in non-modified form or including a diGly-ubiquitin trypsin digestion remnant. Tandem

MS spectra were acquired using collision-induced dissociation. Spectra were searched against the human Refseq_V53 database using Mascot, allowing up to 4 missed cleavages and including carbamidomethyl (C), deamidation (NQ), oxidation (M), GlyGly (K) and LeuArgGlyGly (K) as variable modifications.

In vitro ubiquitylated HA-PALB2 (1-103) (50 μ L reactions) was in-gel reduced using DTT, alkylated using 2-chloroacetamide and trypsin digested for 16 h at 37 °C. Digested peptides were mixed with 20 μ L of a mix of 10 unique heavy isotope-labeled N-terminal PALB2 peptides (Table 1, 80-1200 fmol/ μ L per peptide, based on individual peptide sensitivity testing) before loading 6 μ L onto a 12-15 cm fused silica column with pulled tip packed in-house with 3.5 μ m Zorbax C18. Samples were measured on an Orbitrap ELITE (Thermo Scientific, MA, USA) coupled to an Eksigent nanoLC ultra (AB SCIEX, CA, USA). Peptides were eluted from the column using a 180 min period cycle with a linear gradient from 2% to 35% acetonitrile in 0.1% formic acid. Tandem MS spectra were acquired in a data-dependent mode for the top two most abundant and ten N-terminal PALB2 tryptic digest peptides, either in light or heavy isotope-labeled form. Tandem MS spectra were acquired using collision induced dissociation. Spectra were searched against the human Refseq_V53 database using Mascot, allowing up to 2 missed cleavages and including carbamidomethyl (C), deamidation (NQ), oxidation (M), GlyGly (K) and LeuArgGlyGly (K) as variable modifications, after which spectra were manually checked.

His-Ubiquitin pull-down

293 FLIP-IN cells stably expressing His-Ub were transfected with the indicated siRNA and

treated with doxycycline (DOX) for 24hrs to induce Ub expression. Cells were pre-treated with 10 mM N-ethylmaleimide for 30 min and lysed in denaturing lysis buffer (6 M guanidinium-HCl, 0.1 M Na₂HPO₄/NaH₂PO₄, 10 mM Tris-HCl, 5 mM imidazole, 0.01 M β-mercaptoethanol, Complete protease inhibitor cocktail). Lysates were sonicated on ice twice for 10 sec with 1 min break and centrifuged at 15 000 g for 10 min at 4°C. The supernatant was incubated with Ni-NTA-agarose beads (Qiagen) for 4 h at 4°C. Beads were collected by centrifugation, washed once with denaturing lysis buffer, once with wash buffer (8 M Urea, 0.1 M Na₂HPO₄/NaH₂PO₄, 10 mM Tris-HCl, 5 mM imidazole, 0.01 M β-mercaptoethanol, Complete protease inhibitor cocktail), and twice with wash buffer supplemented with 0.1% Triton X-100, and eluted in elution buffer (0.2 M imidazole, 0.15 M Tris-HCl, 30% glycerol, 0.72 M β-mercaptoethanol, 5% SDS) before analysis by SDS-PAGE and immunoblotting.

HR-based repair assays

Parental U2OS cells and U2OS cells stably expressing wild-type CtIP or CtIP-T847E mutant were transfected with the indicated siRNA and the PALB2-KR construct, synchronized with a single thymidine block, treated with doxycycline to induce CtIP expression and subsequently blocked in G1 phase by adding 40 μM Lovastatin. Cells were collected by trypsinization, washed once with PBS and electroporated with 2.5 μg of sgRNA plasmid and 2.5 μg of donor template using the Nucleofector technology (Lonza; protocol X-001). Cells were plated in medium supplemented with 40 μM Lovastatin and grown for 24hrs before flow cytometry analysis.

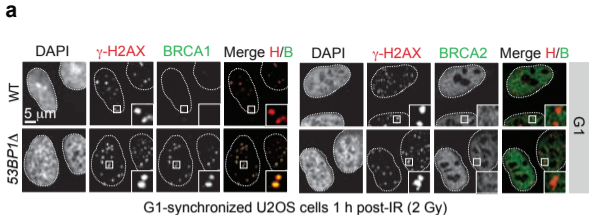
PALB2 chemical ubiquitylation

PALB2 (1-103) polypeptides, engineered with only one cross-linkable cysteine, were ubiquitylated by cross-linking alkylation, as previously described⁴⁰, with the following modifications. Purified PALB2 cysteine mutant (final concentration of 600uM) was mixed with 6xHis-TEV-Ubiquitin G76C (350 μM) in 300 mM Tris pH 8.8, 120 mM NaCl and 5% glycerol. Tris(2-carboxyethyl)phosphine (TCEP) (Sigma-Aldrich) reducing agent was added to a final concentration of 6mM and the mixture and incubated for 30 minutes at room temperature. The bi-reactive cysteine cross-linker, 1,3-dichloroacetone (Sigma-Aldrich), was dissolved in dimethylformamide and added to the protein mix to a final concentration of 5.25 mM. The reaction was allowed to proceed on ice for 1 hr, before being quenched by the addition of 5 mM β-mercaptoethanol. His₆-TEV-Ubiquitin-conjugated PALB2 was enriched by passing over Ni-NTA-agarose beads (Qiagen).

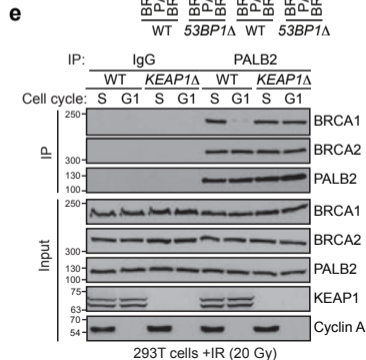
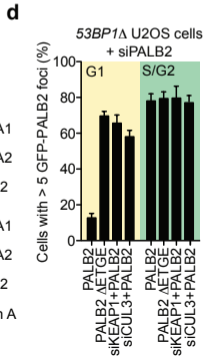
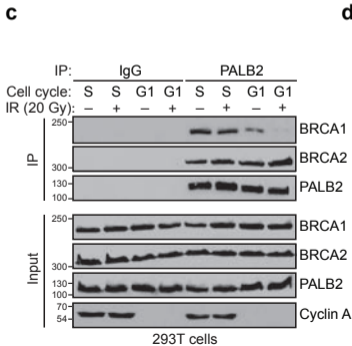
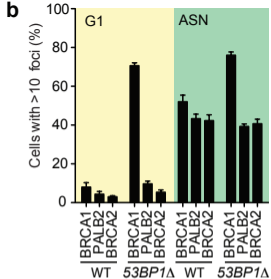
Table 1: Heavy isotope-labeled N-terminal PALB2 tryptic peptides

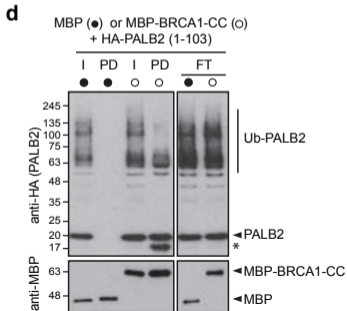
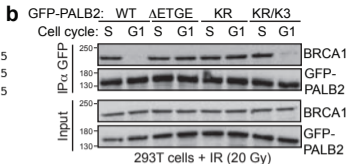
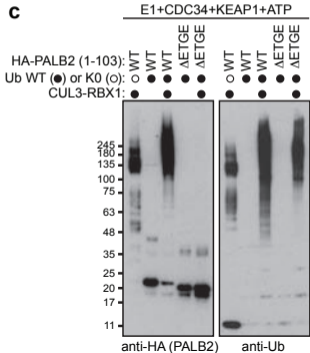
Sequence	Label*	Position in protein	Concentration in final mix	m/z (1+)
EKLKEK	Leu-3	15-20	800 fmol/ μL	781.4891
EK(diG)LKEK	Leu-3	15-20 (K16_ubi)	480 fmol/ μL	895.5321
AQRAEKIK	Arg-3	38-45	800 fmol/ μL	953.5766
AQRAEK(diG)IK	Arg-3	38-45 (K43_ubi)	400 fmol/ μL	1067.6195
LAFLK	Leu-4	21-25	80 fmol/ μL	598.4036
LAFLKR	Leu-4	21-26	800 fmol/ μL	754.5047
LAFLK(diG)R	Leu-4	21-26 (K25_ubi)	80 fmol/ μL	868.5477
EYSK	Lys-4	27-30	1200 fmol/ μL	534.265
EYSKTLAR	Leu-6	27-34	80 fmol/ μL	974.5379
EYSK(diG)TLAR	Leu-6	27-34 (K30_ubi)	80 fmol/ μL	1088.5808

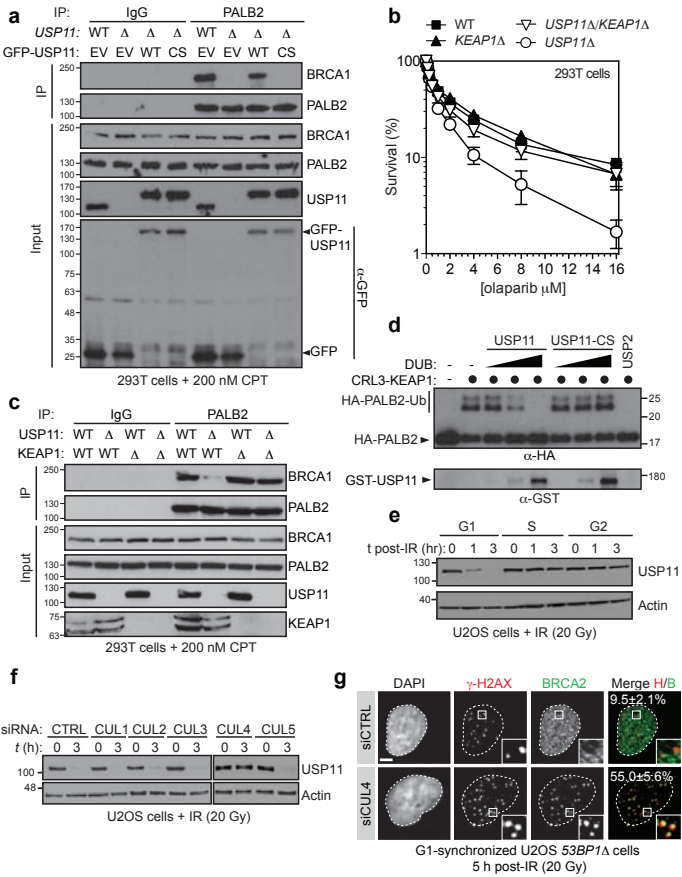
* Labels used: ¹³C¹⁵N-Arginine, ¹³C¹⁵N-Leucine, ¹³C¹⁵N-Lysine

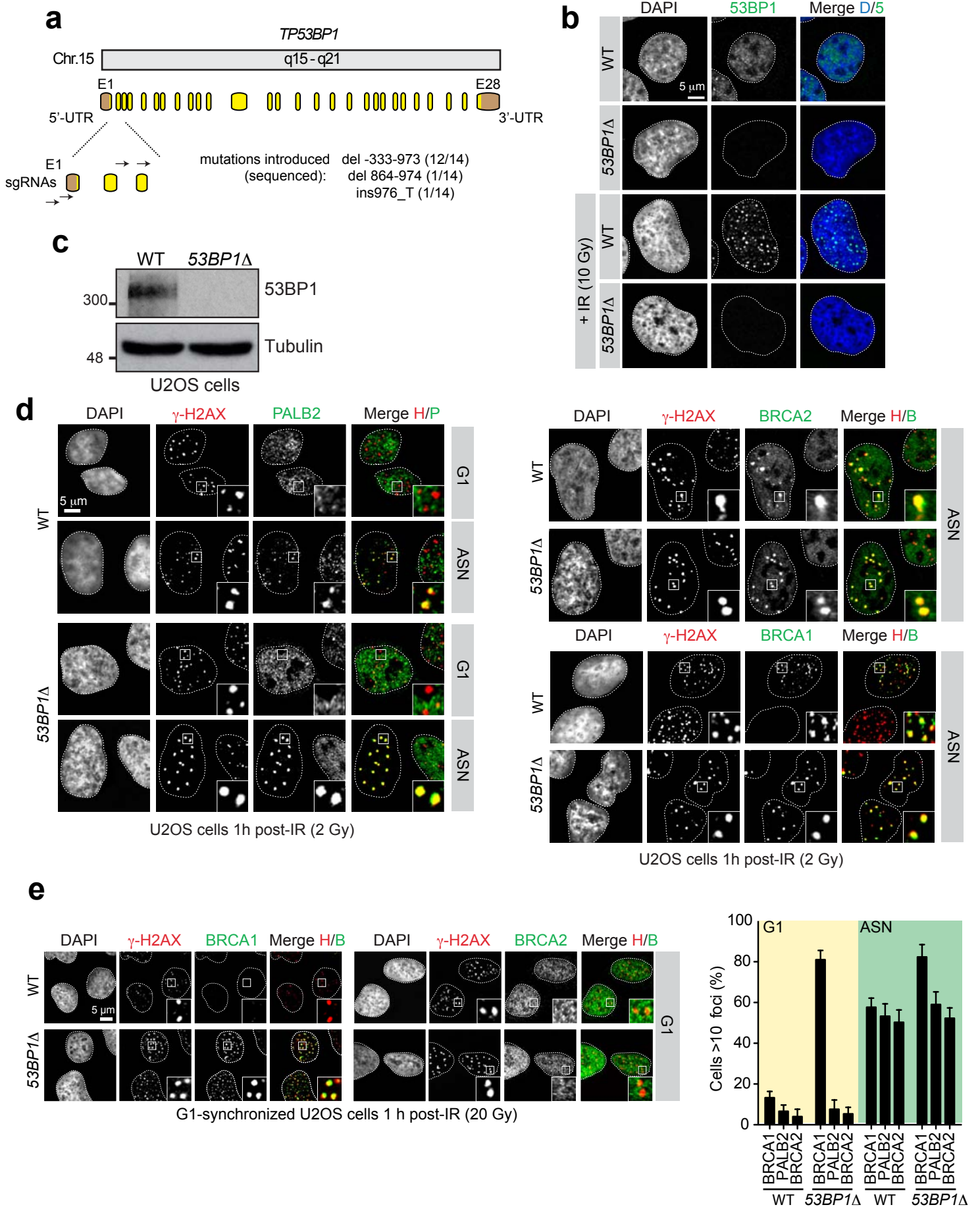


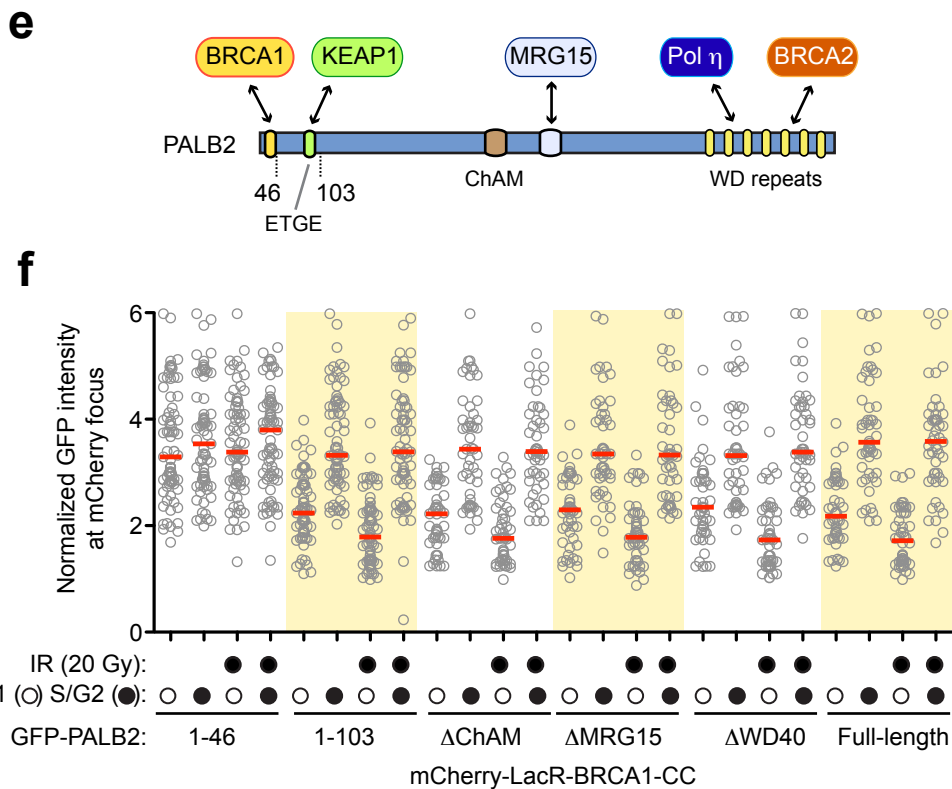
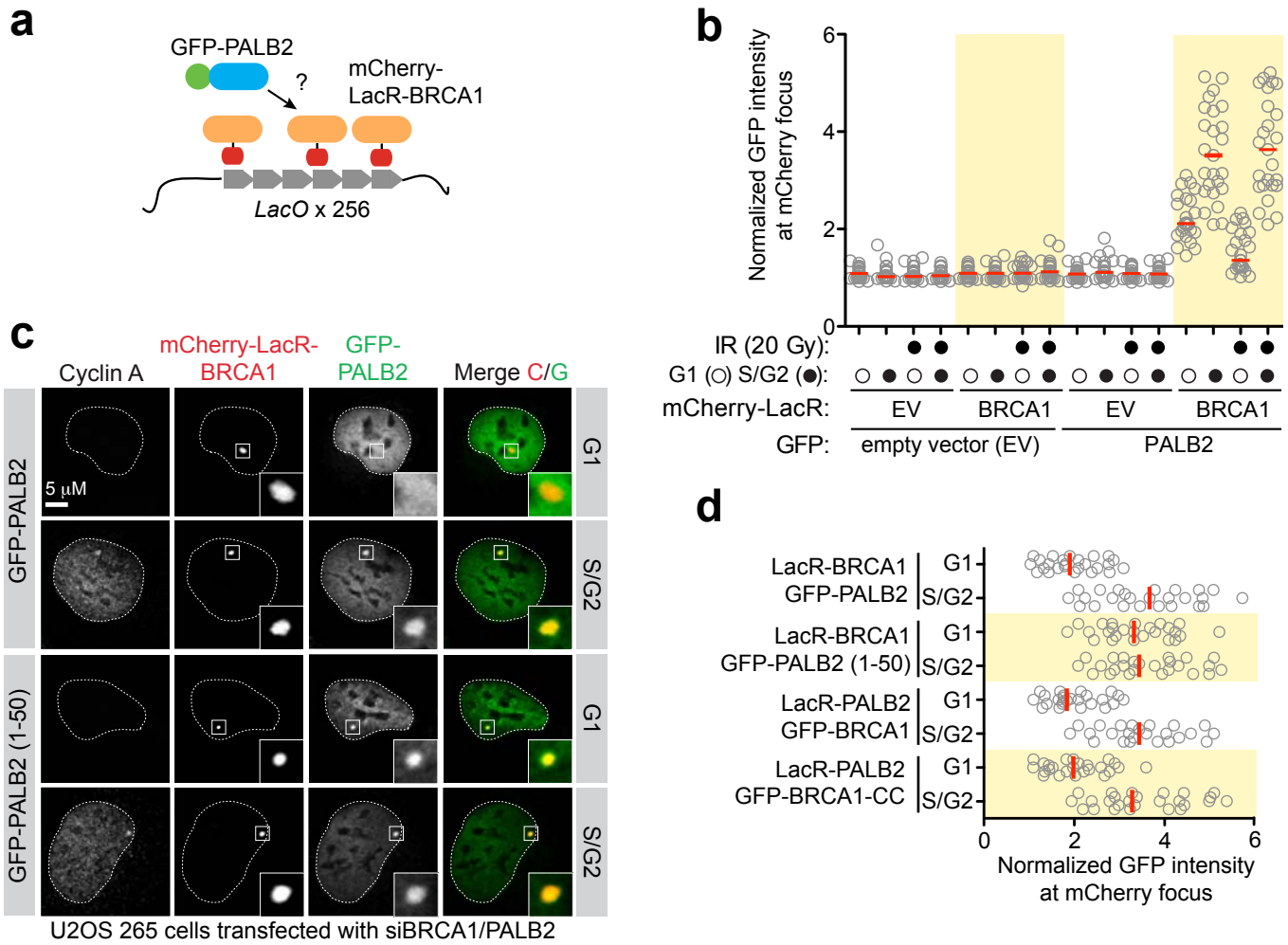
G1-synchronized U2OS cells 1 h post-IR (2 Gy)



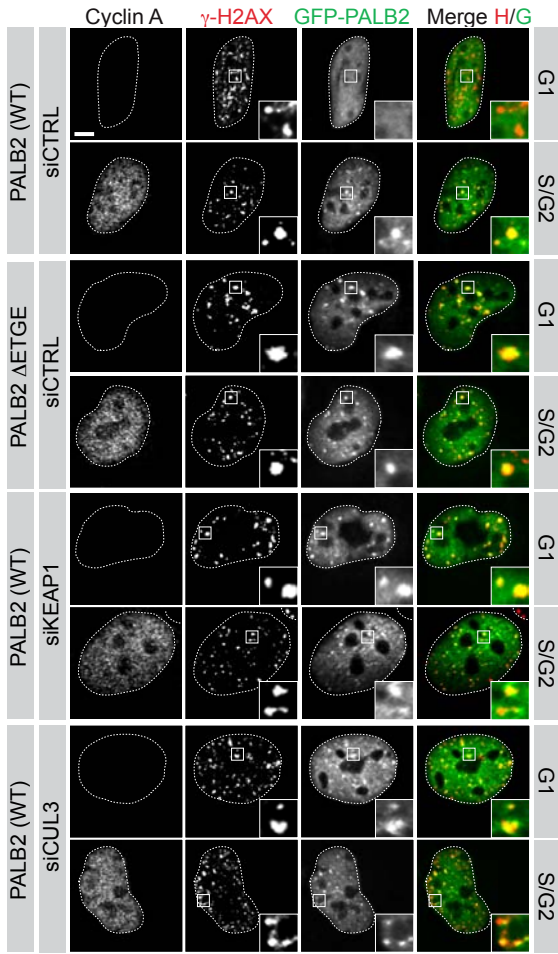






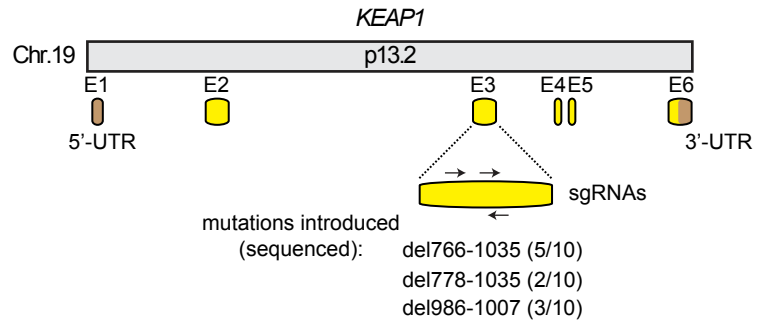


a

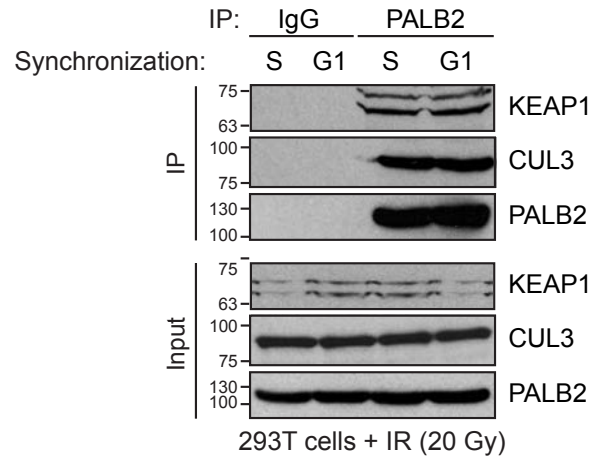


U2OS 53BP1Δ cells 5 h post-IR (20Gy)

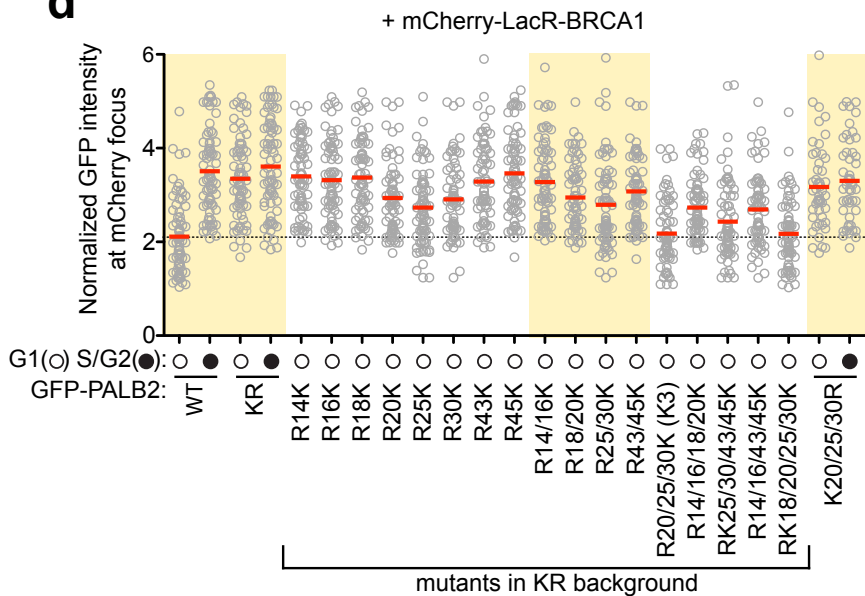
b



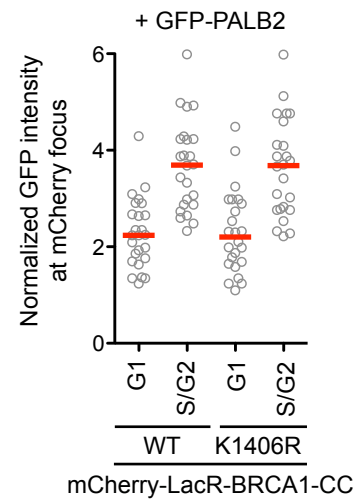
c

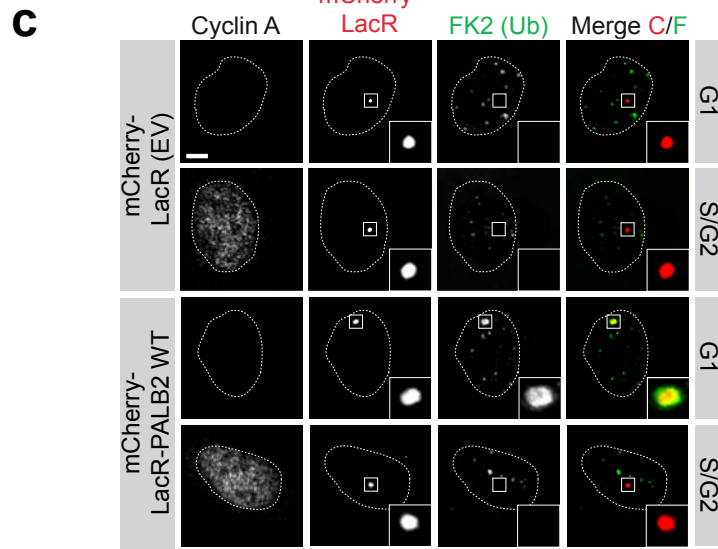
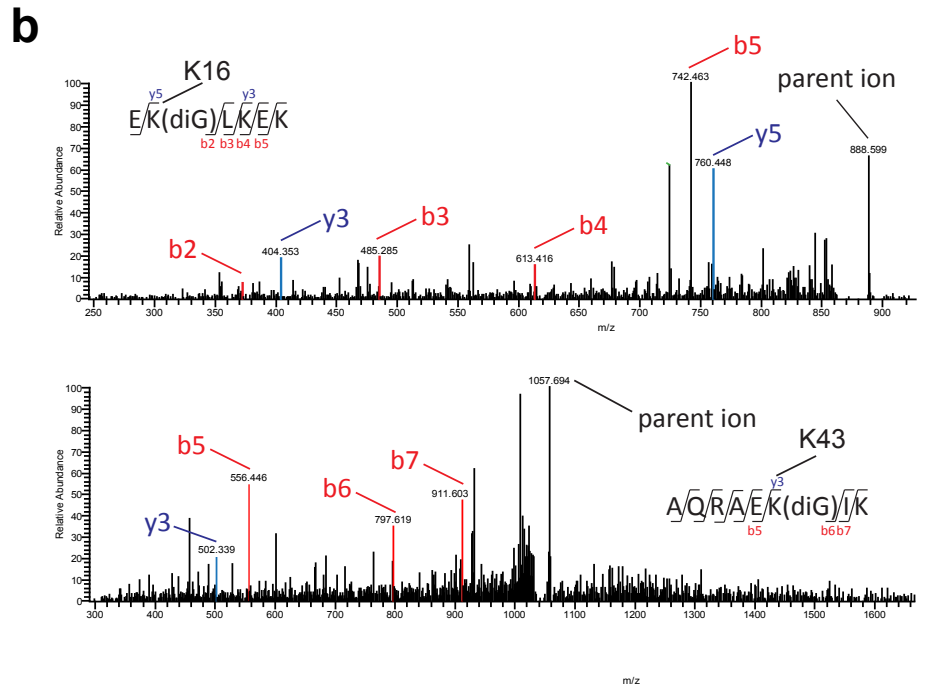
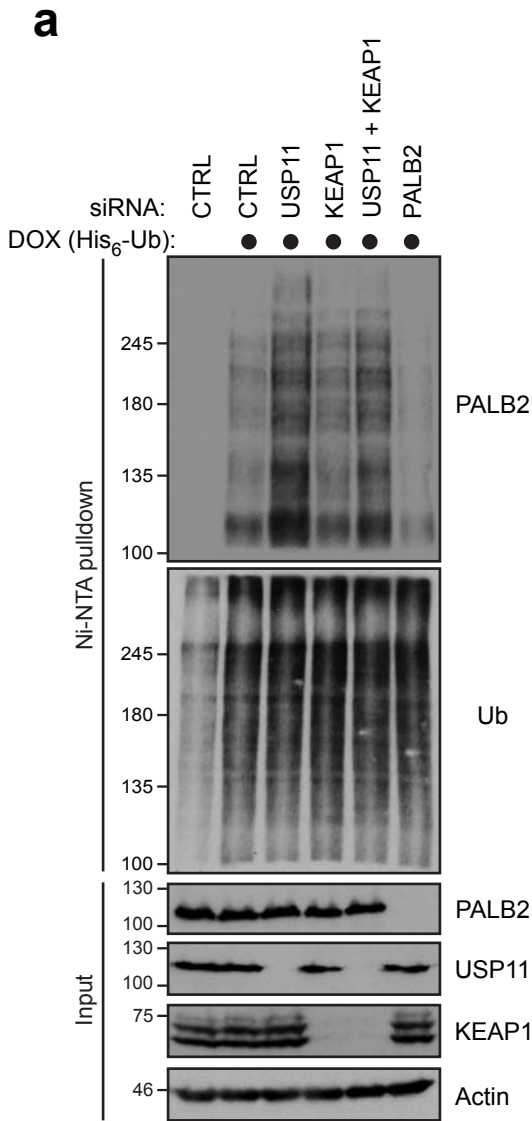


d



e

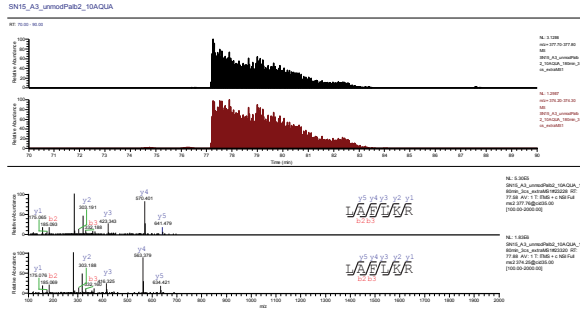




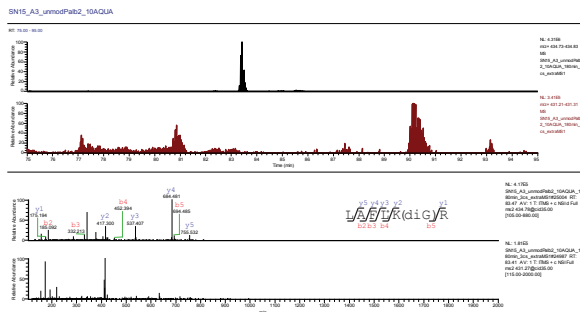
U2OS 256 cells

Control (-CUL3)

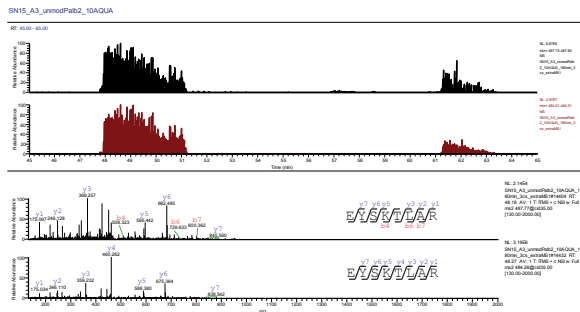
LAFK₂₅R



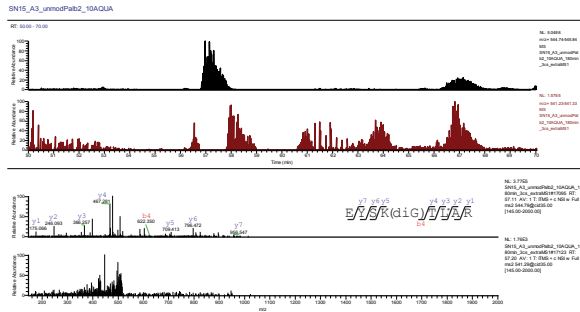
LAFK₂₅(GG)R



EYSK₃₀TLAR

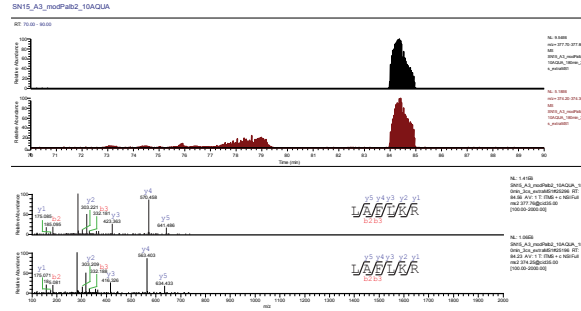


EYSK₃₀(GG)TLAR

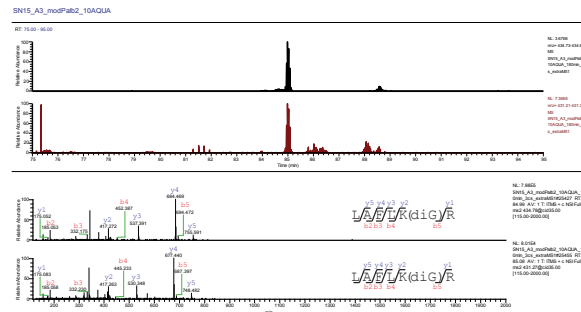


+CUL3

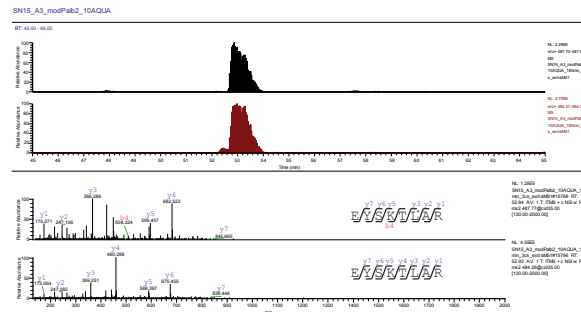
LAFK₂₅R



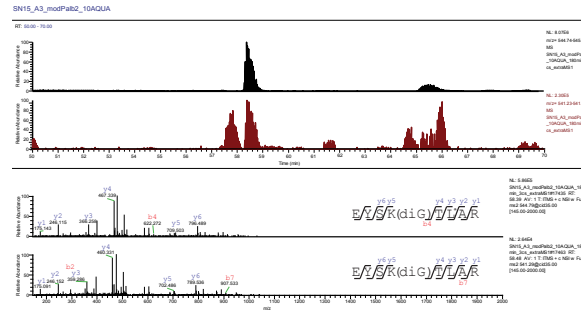
LAFK₂₅(GG)R

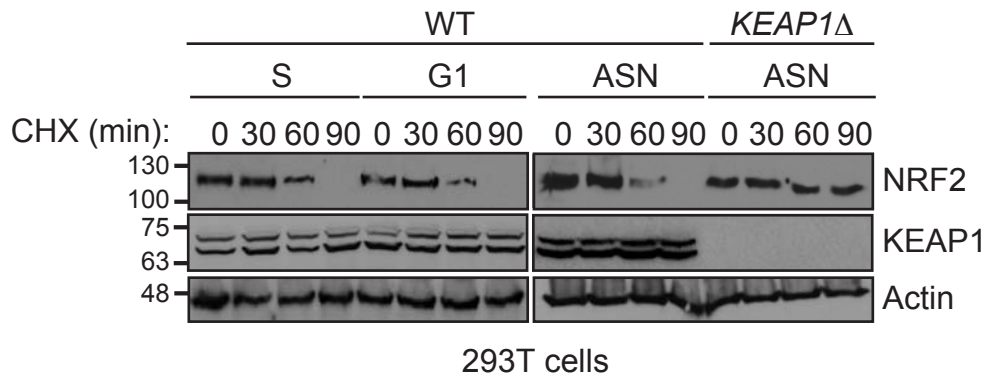


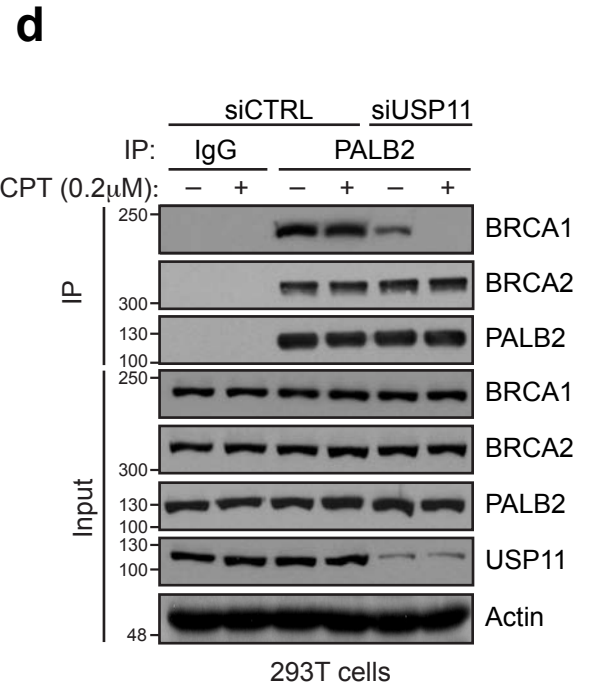
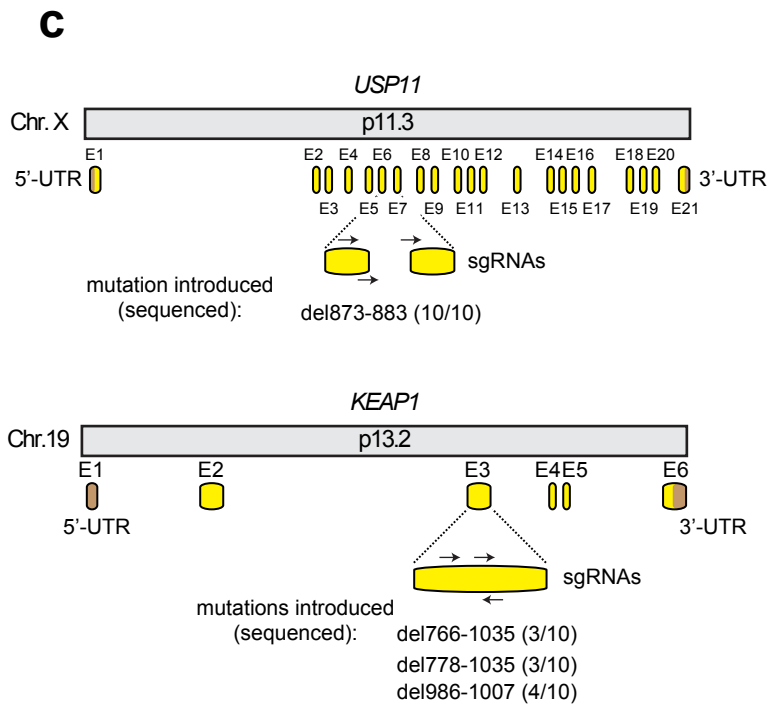
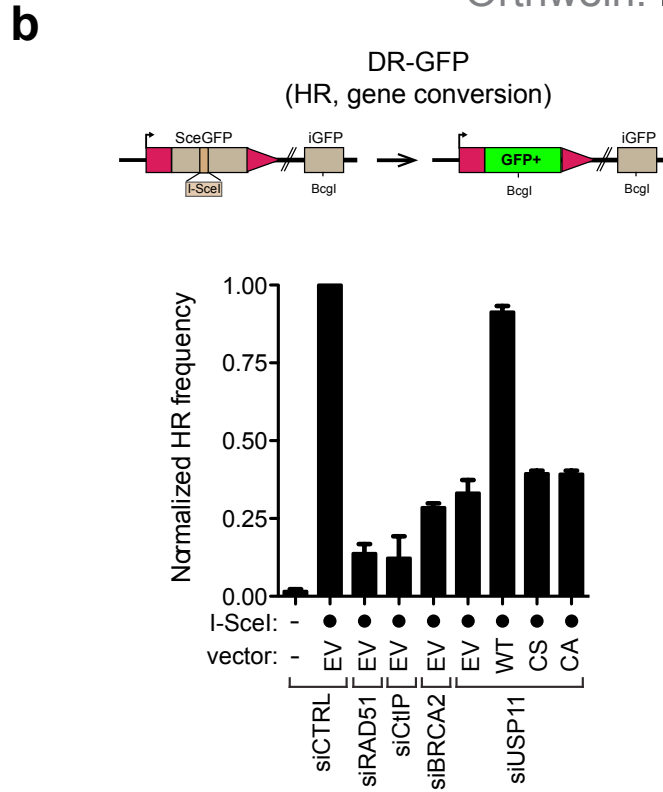
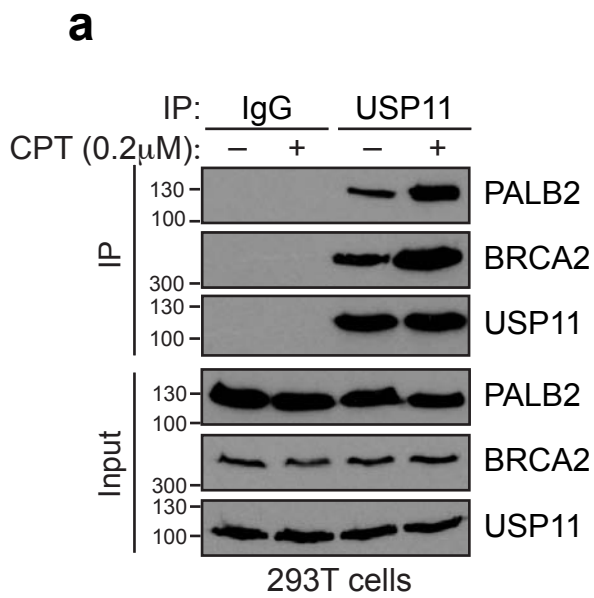
EYSK₃₀TLAR

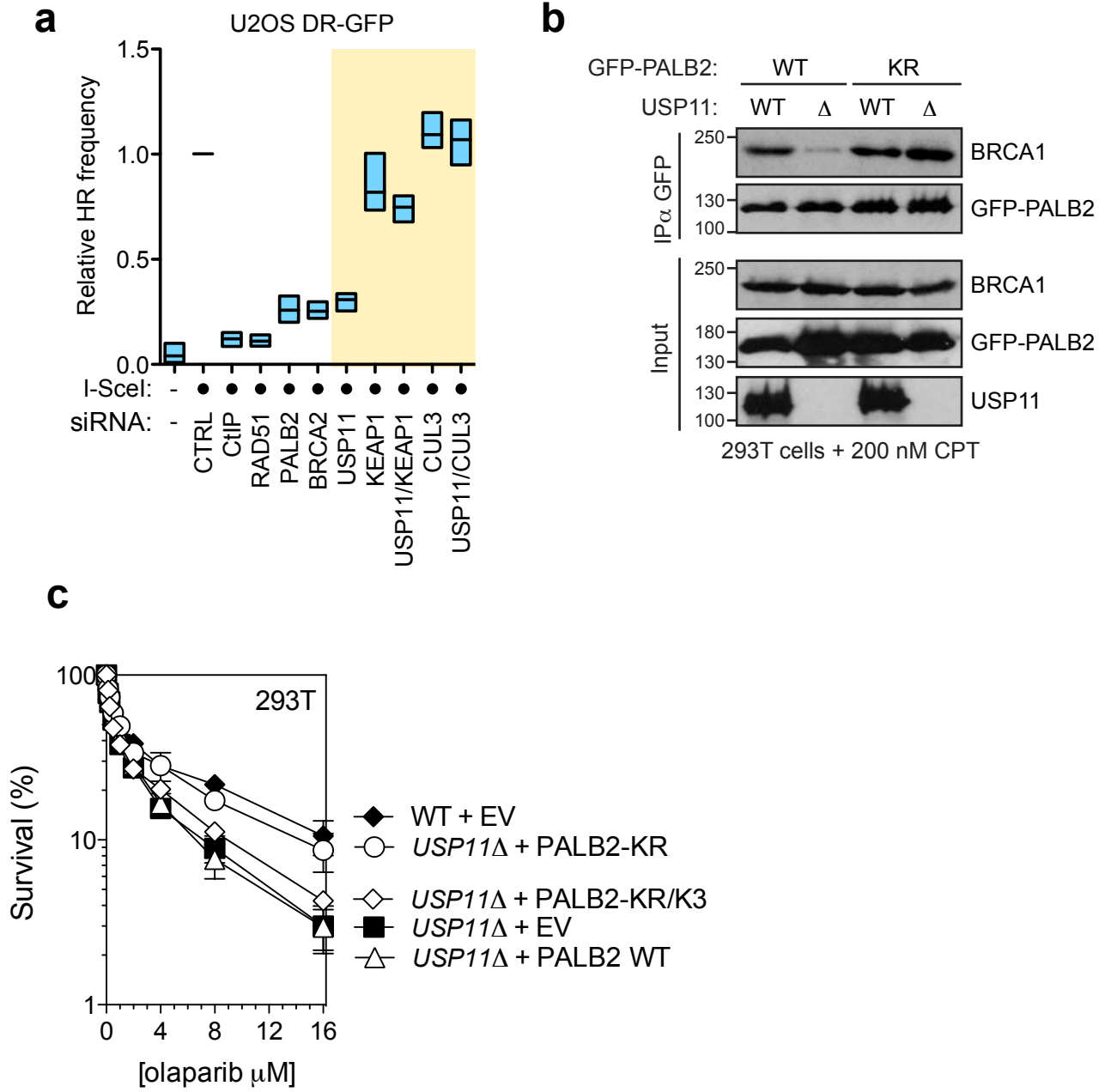


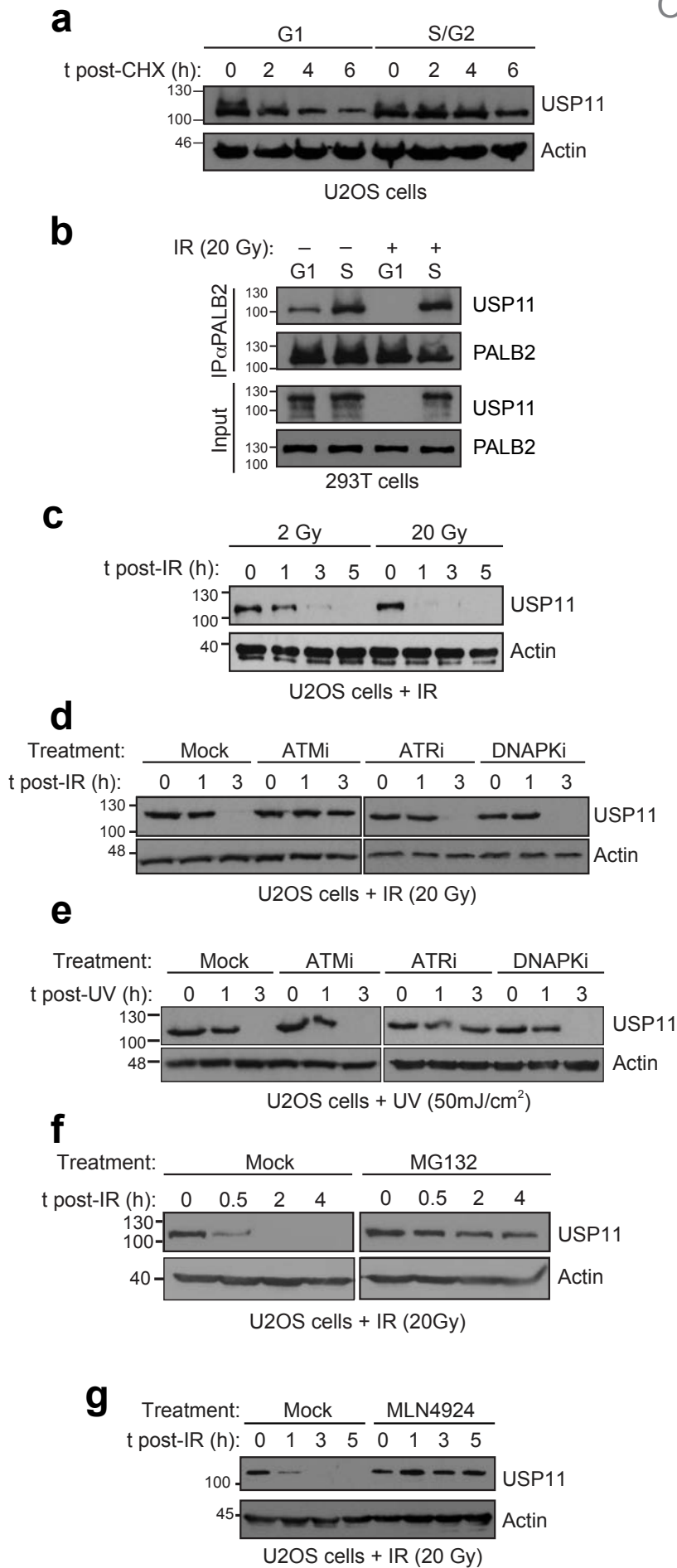
EYSK₃₀(GG)TLAR

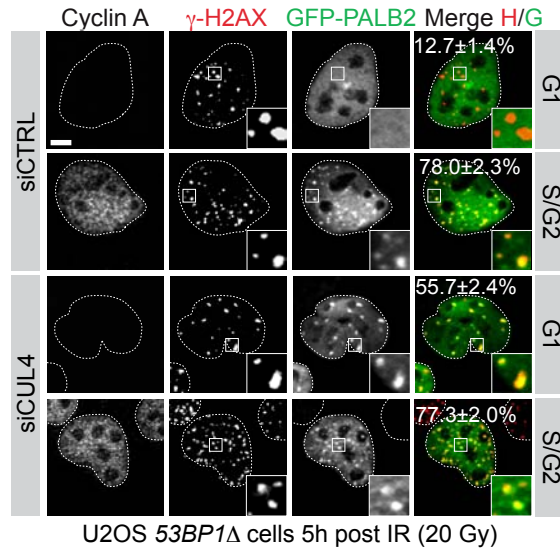


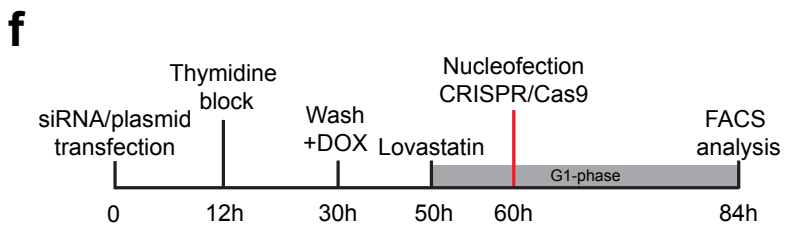
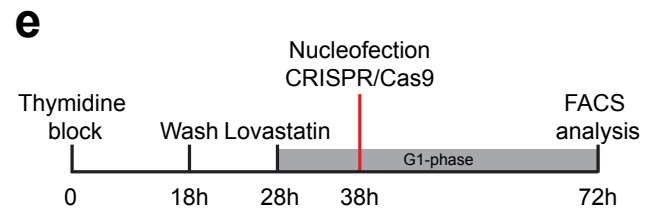
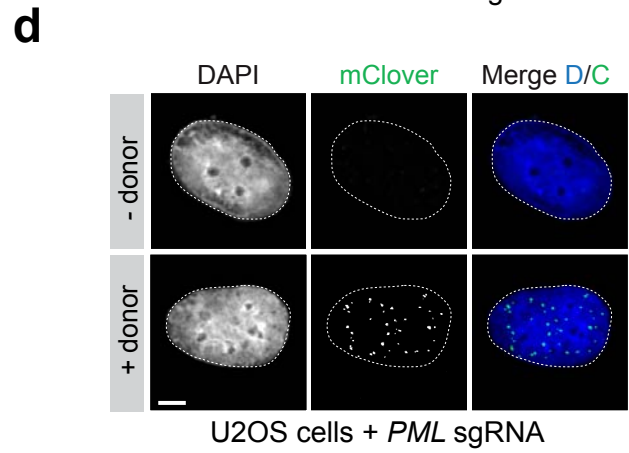
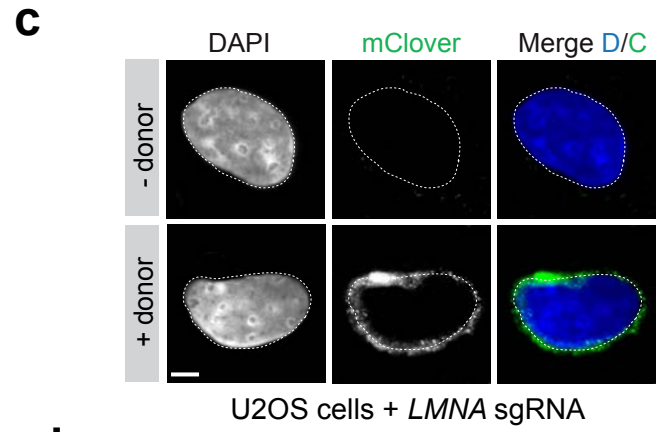
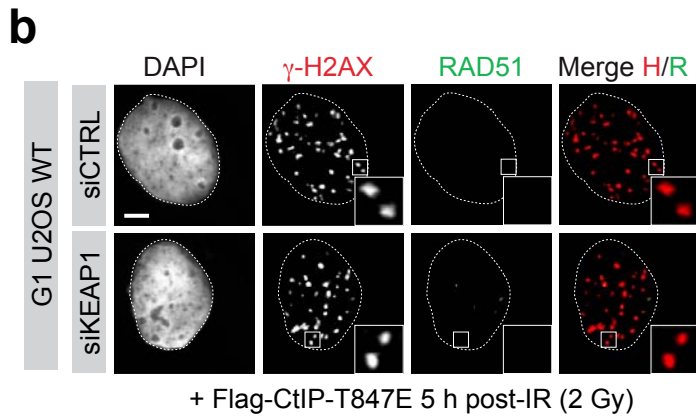
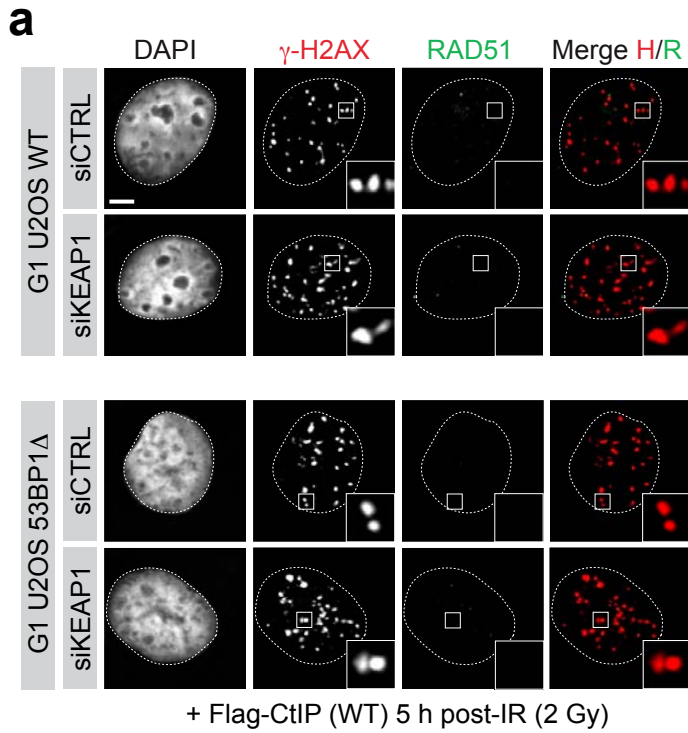


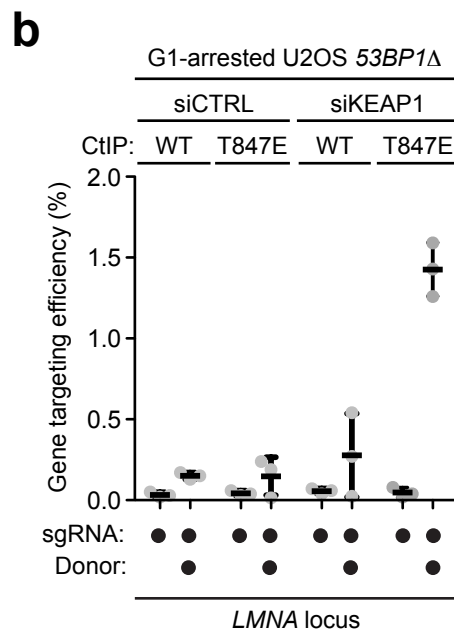
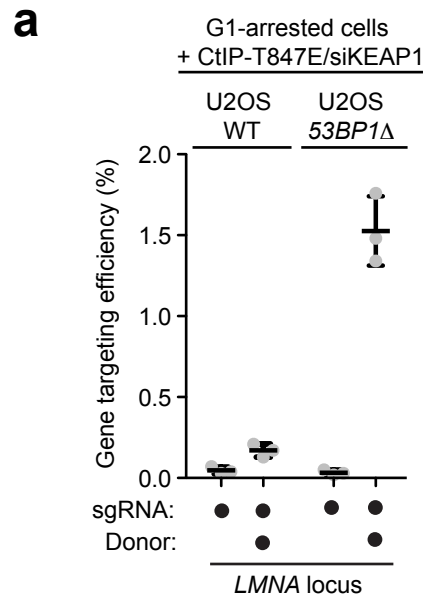












Extended Data Table 1: Heavy isotope-labeled N-terminal PALB2 tryptic peptides

Sequence	Label*	Position in protein	Concentration in final mix	m/z (1+) (heavy labeled)	m/z (1+) (unlabeled)
EKLKEK	Leu-3	15-20	800 fmol/ μ L	781.4891	774.472
EK(diG)LKEK	Leu-3	15-20 (K16_ubi)	480 fmol/ μ L	895.5321	888.5149
AQRAEKIK	Arg-3	38-45	800 fmol/ μ L	953.5766	943.5683
AQRAEK(diG)IK	Arg-3	38-45 (K43_ubi)	400 fmol/ μ L	1067.6195	1057.6113
LAFLK	Leu-4	21-25	80 fmol/ μ L	598.4036	591.3865
LAFLKR	Leu-4	21-26	800 fmol/ μ L	754.5047	747.4876
LAFLK(diG)R	Leu-4	21-26 (K25_ubi)	80 fmol/ μ L	868.5477	861.5305
EYSK	Lys-4	27-30	1200 fmol/ μ L	534.265	526.2508
EYSKTLAR	Leu-6	27-34	80 fmol/ μ L	974.5379	967.5207
EYSK(diG)TLAR	Leu-6	27-34 (K30_ubi)	80 fmol/ μ L	1088.5808	1081.5636

* Labels used: $^{13}\text{C}^{15}\text{N}$ -Arginine, $^{13}\text{C}^{15}\text{N}$ -Leucine, $^{13}\text{C}^{15}\text{N}$ -Lysine